

Temporal nonreciprocity in gently modulated three-mode optomechanical systemsYi-Bing Qian,¹ Zhen-Yu Zhang,¹ Lei Tang ¹, Deng-Gao Lai,² and Bang-Pin Hou ^{1,*}¹*College of Physics and Electronic Engineering, Institute of Solid Physics, Sichuan Normal University, Chengdu 610101, People's Republic of China*²*Theoretical Quantum Physics Laboratory, RIKEN, Saitama 351-0198, Japan*

(Received 31 July 2023; revised 27 February 2024; accepted 15 March 2024; published 3 April 2024)

We investigate temporal dynamics of nonreciprocal photon transmission between two optical modes in a three-mode optomechanical system, where the optical modes are simultaneously driven by two independent periodically amplitude-modulated lasers. We reveal that the nonreciprocal optical transmission oscillating with time can be achieved in the modulated three-mode optomechanical system. By elaborately tuning the strength of the modulation lasers, we can significantly improve the nonreciprocal optical transmission and shorten the convergence time to reach an asymptotic oscillating regime. In particular, the dependence of the temporal photon transmission on the phase difference between two independent amplitude-modulated lasers provides a flexible controllability of optical communication based on optomechanical systems.

DOI: [10.1103/PhysRevA.109.043103](https://doi.org/10.1103/PhysRevA.109.043103)**I. INTRODUCTION**

In general, Lorentz reciprocity refers to the invariant results of measurements when interchanging the positions of source and detector [1]. However, breaking Lorentz reciprocity leads to unique nonreciprocal phenomena, which exhibit a direction-dependent optical transmission. Nonreciprocal devices based on breaking the Lorentz reciprocity, such as isolators and circulators, provide greatly desirable functionalities for quantum information processing, as they can improve information capacity and protect sensitive sources from interfering signals [2]. The optical nonreciprocity serves as a valuable tool in investigating exotic topological photonics [3], achieving the realization of chiral edge states [4], providing topological protection [5], and facilitating ground-state cooling [6].

Traditionally, the optical nonreciprocity is realized by using the magneto-optical materials based on the Faraday rotation effect [7]. Nevertheless, the schemes relying on highly magnetic materials with large magnetic fields are too bulky to be implemented on chip and even deleterious to superconducting devices. To overcome these challenges, many schemes other than those based on the Faraday rotation effect have been proposed to realize nonmagnetic nonreciprocity, such as the Aharonov-Bohm effect in a photonic system [8,9], angular momentum biasing [10,11], chiral quantum networking [12–17], and optical nonlinearity [18–21]. Additionally, the parity-time-symmetric optical structures with balancing gain and loss have been used to realize the nonmagnetic nonreciprocity [22–26].

Recently, cavity optomechanical systems, describing the radiation-pressure induced parametric coupling, have been exploited to achieve the nonmagnetic nonreciprocity due

to their miniaturized and fully integrated features [27–29]. Many interesting phenomena in optomechanical systems have been explored. For example, the optomechanically induced transparency is generated when the optical cavity is driven by a red-detuned field [30–33], while the optomechanically induced absorption and amplification are created when a blue-detuned field is used to drive the cavity [34–37]. To strengthen the quantum features, much attention has been paid to the ground-state cooling of mechanical oscillators [38–42]. In particular, the optomechanical system provides a versatile platform to realize the magnetless nonreciprocity because it can be miniaturized and fully integrated. It was shown that the nonreciprocal photon transmission can be generated in optomechanical systems due to the interference between the multipath coherent couplings [43–54]. This comes from the fact that the constructive interference between different paths can enhance transmission in one direction, but the transmission in the opposite direction is suppressed due to the destructive interference. For example, the nonmagnetic optical nonreciprocity is generated by the interference between the coherent coupling of optical cavities and their optomechanical interactions with the mechanical resonators [48–53]. Additionally, nonreciprocal photon transmission and amplification in the optomechanical systems can be achieved by directly engineering their reservoirs [55–57], or by eliminating auxiliary modes [58–60]. Besides the interference mechanism leading to the nonmagnetic optical nonreciprocity, the nonreciprocity aroused by the optical Sagnac effect has been considered in a spinning optomechanical system [61–63].

Subsequently, several schemes based on the time modulation were proposed to investigate the nonreciprocity. Clerk has proposed the means for inducing a time-independent effective Hamiltonian with a controllable phase in its hopping coupling by modulating the hopping coupling between two modes or their resonance frequencies harmonically in time

*bphou@sicnu.edu.cn

to investigate the nonreciprocity [64]. A giant nonreciprocity was observed by parametrically modulating the resonance frequencies of three identical coupled resonators to lift the degeneracy of counterpropagating resonant states [65]. It was shown that the non-Hermitian time-Floquet system, in which the complex coupling between lossless modes is not only non-Hermitian, but periodic in time, can exhibit perfect nonreciprocity [66].

In the above discussions, the time modulation used for enhancing the nonreciprocity was realized by adjusting the hopping coupling between two modes or their resonance frequencies harmonically in time. Recently, Mari and Eisert have introduced a framework of optomechanical systems that are driven with a mildly amplitude-modulated light field [67]. The squeezing with large degrees of a mechanical micromirror and entanglement dynamics can be achieved in a framework of optomechanical systems that are driven with a mildly amplitude-modulated light field. Subsequently, the mechanical squeezing beyond the rotating wave approximation was analyzed by combining the Lyapunov approach with Floquet techniques for time-dependent problems in optomechanics and electromechanics [68]. And the mode-locked, multimode phonon lasing was established in a multimode optomechanical system through Floquet dynamics induced by a temporally modulated laser drive [69]. Recently, the Floquet control of the optomechanical bistability in multimode settings has been investigated [70]. Additionally, the distinct steady state steered by thermo-optic nonlinearity effects [71], and intriguing dynamics of the high-order sidebands [72–74], can be realized in an optomechanical system. In particular, it was shown that the time-dependent drivings would significantly improve both entanglement and squeezing in coupled optomechanical systems [75–82].

It is natural to wonder how the nonreciprocal transmission behaves in the optomechanical systems driven with mildly amplitude-modulated light fields, which are not subject to classical feedback or squeezed input light. On the other hand, the temporal behaviors (evolution with time) of the quantum system are worth studying, as they not only illustrate the underlying physics structure but also reveal some new features accumulated over time. To our knowledge, the temporal behaviors of the optical nonreciprocity in the optomechanical system, which is periodically driven by gentle amplitude-modulated fields, have not yet been investigated. In the present paper, we consider temporal optical nonreciprocity in an amplitude-modulated three-mode optomechanical system with two independent periodical lasers. The effects of the powers of the zeroth- or first-order modulated driving lasers, their phase difference and modulated frequencies on the temporal nonreciprocal transmission amplitude, and the transition from an initial stage to a steady oscillation with the fixed amplitude in both symmetric and asymmetric settings are investigated by using numerical simulation and analytical findings. In contrast to the previous traveling-wave modulation in the waveguide to produce an isolation (3 dB) and large insertion loss (70 dB) [83], which requires intricate modulation, the present scheme can simplify the nonreciprocal devices by employing a simple periodic modulation of driving fields. This not only reveals the temporal behaviors of the optical nonreciprocity under periodic driving, but provides a

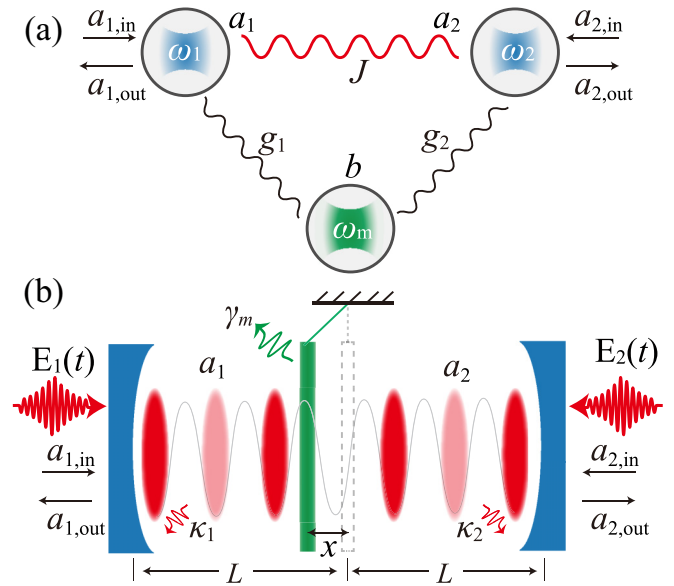


FIG. 1. (a) The three-mode optomechanical system includes common mechanical resonator \hat{b} and two optical cavities \hat{a}_1 and \hat{a}_2 , which are directly coupled with a coherent coupling strength J . (b) Equivalent schematic diagram of the three-mode optomechanical system, consisting of a dielectric membrane as a mechanical resonator, separating an optical cavity into two cavities \hat{a}_1 and \hat{a}_2 . The two optical cavities are coupled with the dielectric membrane \hat{b} via the radiation pressure difference, and tunneling of photons can go through the membrane.

flexible control in dynamical behaviors of the nonreciprocal photon transmission, which may be useful in the real-time photon communications.

This paper is organized as follows: In Sec. II, we introduce the gently modulated three-mode optomechanical systems, in which the optical modes are simultaneously driven by two independent periodically amplitude-modulated lasers. In Sec. III, we obtain the analytical solutions of the mean values by using a perturbation method. We also analyze the dynamical characters of the mean values with both numerical and analytical methods, where the analytical solutions are perfectly consistent with the numerical results. Subsequently, the temporal optical nonreciprocity in the gently modulating three-mode optomechanical systems is discussed by numerical simulation in Sec. IV. And in Sec. V, we study the dependence of temporal nonreciprocal photon transmission on the phase differences. The nonreciprocal behaviors are analytically investigated in Sec. VI. Finally, we summarize our results in Sec. VII.

II. MODEL AND DYNAMICS

As shown in Fig. 1(a), the system under our consideration consists of two optical cavity modes \hat{a}_1 and \hat{a}_2 with frequency ω_{c1} and ω_{c2} , which are optomechanically coupled to a common mechanical mode \hat{b} with frequency ω_m . Meanwhile, the two optical modes are directly coupled with a photon tunneling-coupling strength J . Without loss of generality, we assume that the parameter J is a real number. This three-mode optomechanical systems, which can

be realized in a “membrane-in-the-middle” scheme shown in Fig. 1(b), has been theoretically analyzed [84–86] and experimentally implemented [87–92]. Furthermore, the two cavities are driven by two external input lasers in the opposite directions with carrier frequency ω_l and modulated amplitudes $E_j(t) = E_{j,0} + E_{j,-1}e^{i(\Omega t - \varphi_j)} + E_{j,+1}e^{-i(\Omega t - \varphi_j)}$ ($j = 1, 2$) with φ_j being its initial phase, respectively. And the amplitude of $E_{j,n} = \sqrt{2\kappa P_{j,n}/\hbar\omega_l}$ ($n = 0, \pm 1$) is mainly determined by the power $P_{j,n}$. We shall extend our discussions under the assumption of gentle modulation on the system with $P_{j,1}/P_{j,0} < 1$. The decay rates of the optical cavities are given by $\kappa_i = \pi c/(2F_i L_i)$ ($i = 1, 2$), in which F_i and L_i denote the corresponding cavity finesse and length, respectively, and c is the vacuum speed of light. And $\Omega = 2\pi/\tau$ ($\tau > 0$) is the modulated frequency of the lasers. Under the rotating frame with respect to laser frequencies ω_l , the Hamiltonian of the system reads [67,90] as follows:

$$\begin{aligned} \hat{H} = & \hbar\Delta_1\hat{a}_1^\dagger\hat{a}_1 + \hbar\Delta_2\hat{a}_2^\dagger\hat{a}_2 + \hbar\omega_m\hat{b}^\dagger\hat{b} - \hbar g\hat{a}_1^\dagger\hat{a}_1(\hat{b} + \hat{b}^\dagger) \\ & + \hbar g\hat{a}_2^\dagger\hat{a}_2(\hat{b} + \hat{b}^\dagger) + \hbar J(\hat{a}_1^\dagger\hat{a}_2 + \hat{a}_2^\dagger\hat{a}_1) \\ & + i\hbar\sum_j[E_j(t)\hat{a}_j^\dagger - E_j^*(t)\hat{a}_j], \end{aligned} \quad (1)$$

where $\Delta_j = \omega_{c_j} - \omega_l$ ($j = 1, 2$) is the detuning between the cavity and the corresponding external driving field, \hat{a}_j (\hat{a}_j^\dagger) is the annihilation (creation) operator of the j th cavity mode, and \hat{b} (\hat{b}^\dagger) is the annihilation (creation) operator of the mechanical resonator. And $g = \sqrt{\hbar/m\omega_m\omega_c}/L$ is the single-photon optomechanical-coupling coefficient [27,67], where m is the effective mass of the mechanical mode. The last terms with $E_j(t)$ are periodically modulated drivings on the system.

The Heisenberg-Langevin equations of motion driven by the Hamiltonian in Eq. (1) are given by

$$\begin{aligned} \frac{d}{dt}\hat{b} = & -(i\omega_m + \gamma_m)\hat{b} + ig\hat{a}_1^\dagger\hat{a}_1 - ig\hat{a}_2^\dagger\hat{a}_2 + \sqrt{2\gamma_m}\hat{b}_{\text{in}}, \\ \frac{d}{dt}\hat{a}_1 = & -(i\Delta_1 + \kappa_1)\hat{a}_1 + ig\hat{a}_1(\hat{b} + \hat{b}^\dagger) - iJ\hat{a}_2 \\ & + E_1(t) + \sqrt{2\kappa_1}\hat{a}_{1,\text{in}}, \\ \frac{d}{dt}\hat{a}_2 = & -(i\Delta_2 + \kappa_2)\hat{a}_2 - ig\hat{a}_2(\hat{b} + \hat{b}^\dagger) - iJ\hat{a}_1 \\ & + E_2(t) + \sqrt{2\kappa_2}\hat{a}_{2,\text{in}}, \end{aligned} \quad (2)$$

where γ_m is the mechanical damping rate. Here, $\hat{a}_{1,\text{in}}$, $\hat{a}_{2,\text{in}}$, and \hat{b}_{in} denote the input fields with zero mean values. The spectra $s_{\hat{o},\text{in}}(\omega)$ of the input fields are defined as [46,93]

$$\begin{aligned} \langle \hat{o}_{\text{in}}^\dagger(t')\hat{o}_{\text{in}}(t) \rangle &= 2\pi s_{\hat{o},\text{in}}(t)\delta(t - t'), \\ \langle \hat{o}_{\text{in}}(t)\hat{o}_{\text{in}}^\dagger(t') \rangle &= 2\pi[s_{\hat{o},\text{in}}(t) + 1]\delta(t - t'), \end{aligned} \quad (3)$$

where $\hat{o} = \hat{a}_1, \hat{a}_2$, and \hat{b} , and term 1 results from the effect of vacuum noise. When the system is driven by the strong optical fields, we can linearize the dynamics by using the standard linearization approach of quantum optics, i.e., $\hat{o} = \langle \hat{o} \rangle + \delta\hat{o}$, where $\delta\hat{o}$ are the zero-mean quantum-fluctuation operators around classical c -number mean values $\langle \hat{o} \rangle$. Then the evolution equations of the mean values of the variables can be written as

$$\begin{aligned} \frac{d}{dt}\langle \hat{b} \rangle &= -(i\omega_m + \gamma_m)\langle \hat{b} \rangle + ig|\langle \hat{a}_1 \rangle|^2 - ig|\langle \hat{a}_2 \rangle|^2, \\ \frac{d}{dt}\langle \hat{a}_1 \rangle &= -(i\Delta_1 + \kappa_1)\langle \hat{a}_1 \rangle + ig\langle \hat{a}_1 \rangle(\langle \hat{b} \rangle + \langle \hat{b}^\dagger \rangle) \\ &\quad - iJ\langle \hat{a}_2 \rangle + E_1(t), \\ \frac{d}{dt}\langle \hat{a}_2 \rangle &= -(i\Delta_2 + \kappa_2)\langle \hat{a}_2 \rangle - ig\langle \hat{a}_2 \rangle(\langle \hat{b} \rangle + \langle \hat{b}^\dagger \rangle) \\ &\quad - iJ\langle \hat{a}_1 \rangle + E_2(t). \end{aligned} \quad (4)$$

Correspondingly, the linearized quantum Langevin equations are given by

$$\begin{aligned} \frac{d}{dt}\delta\hat{b} = & -(i\omega_m + \gamma_m)\delta\hat{b} + i(G_1(t)\delta\hat{a}_1^\dagger + G_1^*(t)\delta\hat{a}_1) \\ & - i(G_2(t)\delta\hat{a}_2^\dagger + G_2^*(t)\delta\hat{a}_2) + \sqrt{2\gamma_m}\hat{b}_{\text{in}}, \\ \frac{d}{dt}\delta\hat{a}_1 = & -(i\tilde{\Delta}_1(t) + \kappa_1)\delta\hat{a}_1 + iG_1(t)(\delta\hat{b} + \delta\hat{b}^\dagger) \\ & - iJ\delta\hat{a}_2 + \sqrt{2\kappa_1}\hat{a}_{1,\text{in}}, \\ \frac{d}{dt}\delta\hat{a}_2 = & -(i\tilde{\Delta}_2(t) + \kappa_2)\delta\hat{a}_2 - iG_2(t)(\delta\hat{b} + \delta\hat{b}^\dagger) \\ & - iJ\delta\hat{a}_1 + \sqrt{2\kappa_2}\hat{a}_{2,\text{in}}, \end{aligned} \quad (5)$$

where $\tilde{\Delta}_1 = \Delta_1 - \bar{\delta}$ and $\tilde{\Delta}_2 = \Delta_2 + \bar{\delta}$ with $\bar{\delta} \equiv g(\langle \hat{b}(t) \rangle + \langle \hat{b}^\dagger(t) \rangle)$ are the effective driving detunings including the frequency shifts caused by the optomechanical interaction. The parameters $G_1(t) = g\langle \hat{a}_1(t) \rangle$ and $G_2(t) = g\langle \hat{a}_2(t) \rangle$ represent the effective optomechanical-coupling strength related to the cavity intensity. For convenience, the linearized fluctuation Eq. (5) can be concisely expressed as

$$\frac{d}{dt}\mathbf{v} = \mathbf{A}\mathbf{v} + \mathbf{L}\mathbf{v}_{\text{in}}, \quad (6)$$

where the fluctuation vector is $\mathbf{v} = (\delta\hat{b}, \delta\hat{a}_1, \delta\hat{a}_2, \delta\hat{b}^\dagger, \delta\hat{a}_1^\dagger, \delta\hat{a}_2^\dagger)^T$, and the input field vector is $\mathbf{v}_{\text{in}} = (\hat{b}_{\text{in}}, \hat{a}_{1,\text{in}}, \hat{a}_{2,\text{in}}, \hat{b}_{\text{in}}^\dagger, \hat{a}_{1,\text{in}}^\dagger, \hat{a}_{2,\text{in}}^\dagger)^T$ with decay matrix $\mathbf{L} = \text{diag}(\sqrt{2\gamma_m}, \sqrt{2\kappa_1}, \sqrt{2\kappa_2}, \sqrt{2\gamma_m}, \sqrt{2\kappa_1}, \sqrt{2\kappa_2})$. The coefficient matrix \mathbf{A} is given by

$$\mathbf{A} = \begin{pmatrix} -(i\omega_m + \gamma_m) & iG_1^*(t) & -iG_2^*(t) & 0 & iG_1(t) & -iG_2(t) \\ iG_1(t) & -(i\tilde{\Delta}_1(t) + \kappa_1) & -iJ & iG_1(t) & 0 & 0 \\ -iG_2(t) & -iJ & -(i\tilde{\Delta}_2(t) + \kappa_2) & -iG_2(t) & 0 & 0 \\ 0 & -iG_1^*(t) & iG_2^*(t) & i\omega_m - \gamma_m & -iG_1(t) & iG_2(t) \\ -iG_1^*(t) & 0 & 0 & -iG_1^*(t) & i\tilde{\Delta}_1(t) - \kappa_1 & iJ \\ iG_2^*(t) & 0 & 0 & iG_2^*(t) & iJ & i\tilde{\Delta}_2(t) - \kappa_2 \end{pmatrix}. \quad (7)$$

The stability of this optomechanical system can be influenced by the gently modulated lasers. According to the Routh-Hurwitz criterion [94], the dynamics of the system is stable when all eigenvalues of the matrix (7) have a negative real part. However, the corresponding expressions indicating the stability of the system are too cumbersome to be shown here. We have verified that the parameter values considered here fulfill the stability condition.

III. DYNAMIC CHARACTERS OF THE MEAN VALUES

The time evolution of the mean values is crucial for studying the dynamic characters of the quantum fluctuations, shown in Eq. (4). By introducing the dimensionless position and momentum quadratures of the mechanical mode $\hat{q} = (\hat{b} + \hat{b}^\dagger)/\sqrt{2}$, and $\hat{p} = -i(\hat{b} - \hat{b}^\dagger)/\sqrt{2}$, the time evolution of the mean values in Eq. (4) can be rewritten as

$$\begin{aligned} \frac{d}{dt}\langle\hat{a}_1\rangle &= -(i\Delta_1 + \kappa_1)\langle\hat{a}_1\rangle + i\sqrt{2}g\langle\hat{a}_1\rangle\langle\hat{q}\rangle - iJ\langle\hat{a}_2\rangle + E_1(t), \\ \frac{d}{dt}\langle\hat{a}_2\rangle &= -(i\Delta_2 + \kappa_2)\langle\hat{a}_2\rangle - i\sqrt{2}g\langle\hat{a}_2\rangle\langle\hat{q}\rangle - iJ\langle\hat{a}_1\rangle + E_2(t), \\ \frac{d}{dt}\langle\hat{p}\rangle &= -\omega_m\langle\hat{q}\rangle + \sqrt{2}g|\langle\hat{a}_1\rangle|^2 - \sqrt{2}g|\langle\hat{a}_2\rangle|^2 - \gamma_m\langle\hat{p}\rangle, \\ \frac{d}{dt}\langle\hat{q}\rangle &= \omega_m\langle\hat{p}\rangle - \gamma_m\langle\hat{q}\rangle. \end{aligned} \quad (8)$$

In general, Eq. (8) is nonlinear and difficult to find the exact solutions directly. However, when the system is far away from instabilities and multistabilities [67,79,81], the gently modulated field can be regard as a perturbation term. Therefore, the asymptotic solutions of the mean values are expected to have the same periodicity τ of the modulated field $E_j(t + \tau) = E_j(t)$. In particular, it is reasonable to perform a double Fourier expansion for the mean value $\langle\hat{\delta}(t)\rangle$ in the power of the optomechanical-coupling constant $\sqrt{2}g$, i.e.,

$$\langle\hat{\delta}(t)\rangle = \sum_{l=0}^{\infty} \sum_{n=-\infty}^{\infty} o^{n,l} e^{in\Omega t} (\sqrt{2}g)^l. \quad (9)$$

Correspondingly, the periodically modulated amplitude $E_j(t)$ ($j = 1, 2$) can be expressed as

$$E_j(t) = \sum_{n=-\infty}^{\infty} E_{j,n} e^{in\Omega t}, \quad (10)$$

where $\Omega = 2\pi/\tau$ is the fundamental modulation frequency. By substituting Eqs. (9) and (10) into Eq. (8), we can get the time-independent coefficients $o^{n,0}$, given by

$$\begin{aligned} q^{n,0} &= 0, p^{n,0} = 0, \\ a_1^{0,0} &= \frac{(\kappa_2 + i\Delta_2)E_{1,0} - iJE_{2,0}}{J^2 + (\kappa_1 + i\Delta_1)(\kappa_2 + i\Delta_2)}, \\ a_2^{0,0} &= \frac{(\kappa_1 + i\Delta_1)E_{2,0} - iJE_{1,0}}{J^2 + (\kappa_1 + i\Delta_1)(\kappa_2 + i\Delta_2)}, \\ a_1^{\pm 1,0} &= \frac{e^{\mp i\varphi_2} \{[\kappa_2 + i(\Delta_2 \pm \Omega)]E_{1,\mp 1} e^{\mp i\varphi} - iJE_{2,\mp 1}\}}{J^2 + [\kappa_1 + i(\Delta_1 \pm \Omega)][\kappa_2 + i(\Delta_2 \pm \Omega)]}, \\ a_2^{\pm 1,0} &= \frac{e^{\mp i\varphi_2} \{[\kappa_1 + i(\Delta_1 \pm \Omega)]E_{2,\mp 1} - iJE_{1,\mp 1} e^{\mp i\varphi}\}}{J^2 + [\kappa_1 + i(\Delta_1 \pm \Omega)][\kappa_2 + i(\Delta_2 \pm \Omega)]}, \end{aligned} \quad (11)$$

where $\varphi = \varphi_1 - \varphi_2$ is the phase difference between the two modulated lasers. The zeroth-order perturbation ($l = 0$) with respect to $\sqrt{2}g$ is given by $a_j^{n,0} = 0$ for $n \neq 0, \pm 1$. Also, we can get the following recursive relations of the coefficients $o^{n,l}$ for $l \geq 1$:

$$\begin{aligned} p^{n,l} &= \frac{in\Omega + \gamma_m}{\omega_m} q^{n,l}, \\ q^{n,l} &= \omega_m \sum_{k=0}^{l-1} \sum_{m=-\infty}^{\infty} \frac{(a_1^{m,k})^* a_1^{n+m,l-k-1} - (a_2^{m,k})^* a_2^{n+m,l-k-1}}{\omega_m^2 + (in\Omega + \gamma_m)^2}, \\ a_1^{n,l} &= i \sum_{k=0}^{l-1} \sum_{m=-\infty}^{\infty} \frac{a_1^{m,k} q^{n-m,l-k-1} - Ja_2^{n,l}}{\kappa_1 + i(\Delta_1 + n\Omega)}, \\ a_2^{n,l} &= -i \sum_{k=0}^{l-1} \sum_{m=-\infty}^{\infty} \frac{a_2^{m,k} q^{n-m,l-k-1} + Ja_1^{n,l}}{\kappa_2 + i(\Delta_2 + n\Omega)}. \end{aligned} \quad (12)$$

By truncating the series to the terms with $j \leq 10$ and $n = -1, 0, 1$, we find that the obtained analytical approximations for the asymptotic mean values $\langle\hat{\delta}(t)\rangle$ exhibit excellent consistency with the numerical results. This is further confirmed by comparing the time evolution of the mean values of the cavity fields by truncating the series at $l = 10$ in Eq. (12) with those for the case of $l \leq 12$, which is not shown here. Thus, it becomes convenient to evaluate the linearized quantum dynamics with a good enough degree of accuracy by using the truncated Fourier expansions in Eq. (9). In order to make the following results within experimental realizations, we use the parameters from the state-of-the-art experiments [27,67]: $L = 25$ mm, $m = 150$ ng, $F = 1.4 \times 10^4$, $Q = \omega_m/\gamma_m = 10^5$, $\omega_m = 2\pi \times 10^6$ Hz, $\kappa = 2\pi \times 215$ kHz, $T = 0.1$ K, and $\lambda = 1064$ nm. Additionally, the two cavities are driven under red-sideband resonance with $\Delta_1 = \Delta_2 = \omega_m$ with a small sinusoidal modulation frequency being $\Omega/\omega_m = 2$.

The time evolution of the mean values $n_1(t) = \langle\hat{a}_1^\dagger(t)\hat{a}_1(t)\rangle$ (red solid lines) and $n_2(t) = \langle\hat{a}_2^\dagger(t)\hat{a}_2(t)\rangle$ (blue solid line) for the different phase difference $\varphi = 0, 0.4\pi, \pi$, and -0.4π is shown Fig. 2. It indicates that the results of numerical simulations (solid lines) for the time evolution of the mean values are consistent with those of analytical results in the long-time limit, which further verifies the accuracy and reasonability of our discussions. Specifically, in Fig. 2(a) we see that in the case of symmetric modulations with their amplitudes of $E_1(t) = E_2(t)$ and the red-sideband resonance $\Delta_1 = \Delta_2 = \omega_m$, the asymptotic periodic evolution of the cavity field $n_1(t)$ exhibits the limit-cycle oscillation and synchronizes with the field $n_2(t)$, which agrees well with the results shown in Refs. [79,81,82]. The synchronized evolutions of the two classical fields $n_j(t) = \langle\hat{a}_j^\dagger(t)\hat{a}_j(t)\rangle$ ($j = 1, 2$) can be illustrated by the expressions in Eqs. (11) and (12) in detail, which are given by

$$\begin{aligned} q^{n,0} &= p^{n,0} = 0, \\ a_1^{0,0} &= a_2^{0,0} = \frac{\kappa + i\omega_m - iJ}{J^2 + (\kappa + i\omega_m)^2} E_{1(2),0}, \\ a_1^{\pm 1,0} &= a_2^{\pm 1,0} = \frac{\kappa + i(\omega_m \pm \Omega) - iJ}{J^2 + [\kappa + i(\omega_m \pm \Omega)]^2} E_{1(2),\mp 1}(t) e^{\mp i\varphi_2}, \\ p^{n,l} &= q^{n,l} = a_1^{n,l} = a_2^{n,l} = 0. \end{aligned} \quad (13)$$

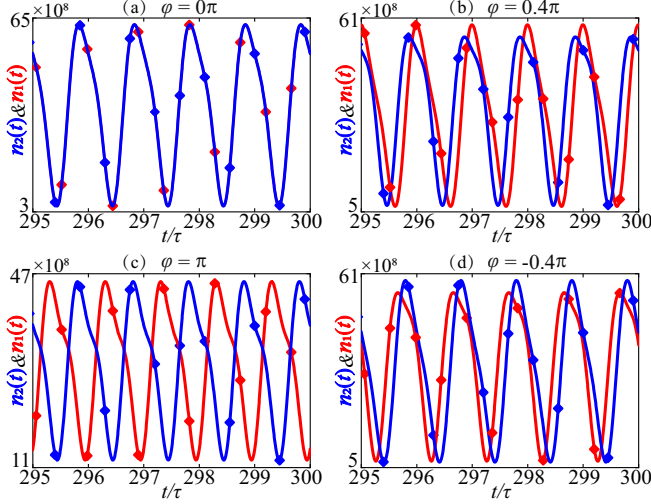


FIG. 2. (a)–(d) Time evolution of the mean values of the cavity fields $n_1(t) = \langle \hat{a}_1^\dagger(t)\hat{a}_1(t) \rangle$ (red solid lines) and $n_2(t) = \langle \hat{a}_2^\dagger(t)\hat{a}_2(t) \rangle$ (blue solid lines) for different phases φ : (a) $\varphi = 0$, (b) $\varphi = 0.4\pi$, (c) $\varphi = \pi$, and (d) $\varphi = -0.4\pi$. All the lines are based on the numerical solutions with Eq. (8) and the markers correspond to the analytical solutions Eqs. (11) and (12). Other parameters are $J/\kappa = 1$, $P_{1,0} = P_{2,0} = 10$ mW, $P_{1,\pm 1} = P_{2,\pm 1} = 2.2$ mW, and $\kappa_1 = \kappa_2 = \kappa$.

Furthermore, the synchronized behaviors of the fields $n_1(t)$ and $n_2(t)$ are remarkably dependent on the phase difference φ . The synchronized state can be broken when the phase difference φ is not equal to zero, as demonstrated in Figs. 2(b)–2(d). If the phase difference is set as $\varphi = \pi$ in Fig. 2(c), $n_1(t)$ and $n_2(t)$ oscillate in an antiphase synchronization state with a period of $\tau = 2\pi/\Omega$. In addition, it is shown that the maximum value of $n_1(t)$ is greater than that of $n_2(t)$ at $\varphi = 0.4\pi$ in Fig. 2(b), while it is smaller than that of $n_2(t)$ at $\varphi = -0.4\pi$ in Fig. 2(d). Therefore, the comparison of these figures implies that the synchronized state and their oscillating strengths of $n_1(t)$ and $n_2(t)$ can be flexibly controlled by adjusting the phase difference φ .

IV. TEMPORAL NONRECIPROCAL PHOTON TRANSMISSION

Now, we shall investigate the temporal nonreciprocal transmission in the three-mode optomechanical systems under the periodical drivings of the amplitude-modulated lasers. Without loss of generality, we assume that the optomechanical coupling with the forward input $\hat{a}_{1,\text{in}}$ and that with the backward input $\hat{a}_{2,\text{in}}$ are identical: $\kappa_1 = \kappa_2$. We neglect the cavity intrinsic loss and consider the case of overcoupled cavities with $\kappa_{\text{ex},j} = \kappa_j$, ($j = 1, 2$). Based on the standard input-output relation [95], the amplitude of the output field $\delta\hat{a}_{j,\text{out}}$ is related to the corresponding cavity field $\delta\hat{a}_j$ as follows: $\delta\hat{a}_{j,\text{out}} = \sqrt{2\kappa_j}\delta\hat{a}_j - \delta\hat{a}_{j,\text{in}}$, ($j = 1, 2$). According to Eq. (6), the output amplitude at the \hat{a}_2 port is described by $\delta\hat{a}_{2,\text{out}} = \sqrt{2\kappa_2}\delta\hat{a}_2$ in the case of the forward photon transmission from \hat{a}_1 to \hat{a}_2 ($\hat{a}_{1,\text{in}} \neq 0$ and $\hat{a}_{2,\text{in}} = 0$). Similarly, the output amplitude at the \hat{a}_1 port is given by $\delta\hat{a}_{1,\text{out}} = \sqrt{2\kappa_1}\delta\hat{a}_1$ for the backward transmission from \hat{a}_2 to \hat{a}_1

($\hat{a}_{1,\text{in}} = 0$ and $\hat{a}_{2,\text{in}} \neq 0$). Accordingly, transmissions coefficients in the forward and backward directions are defined as $T_{1 \rightarrow 2} = 2\kappa_2|\delta\hat{a}_2/\hat{a}_{1,\text{in}}|^2$ and $T_{2 \rightarrow 1} = 2\kappa_1|\delta\hat{a}_1/\hat{a}_{2,\text{in}}|^2$, respectively.

To show the temporal nonreciprocity between the two optical modes \hat{a}_1 and \hat{a}_2 , we plot the transmissions coefficients versus the normalized time t/τ for the different powers of modulated driving laser $P_{1,\pm 1} = P_{2,\pm 1} = 2.2, 2.4$, and 2.6 mW with a fixed zeroth-order modulated laser $P_{1,0} = P_{2,0} = 10$ mW in Fig. 3, where the red and blue curves correspond to the transmission coefficients of $T_{1 \rightarrow 2}$ and $T_{2 \rightarrow 1}$, respectively. We find that there exists a temporal nonreciprocal transmission between \hat{a}_1 and \hat{a}_2 , which periodically oscillates with time. It is shown in Fig. 3(a) for $P_{1,\pm 1} = P_{2,\pm 1} = 2.2$ mW that the amplitude of $T_{1 \rightarrow 2} \approx 1.6$ is larger than $T_{2 \rightarrow 1} \approx 0.32$ around $t = 50\tau$. As the strength of the powers of the modulated driving lasers increases, the temporal nonreciprocity is more effective. In Fig. 3(b) for $P_{1,\pm 1} = P_{2,\pm 1} = 2.2$ mW, we can get that the amplitude of $T_{1 \rightarrow 2} \approx 6.8$ is much larger than $T_{2 \rightarrow 1} \approx 0.92$ within the steady oscillation region.

On the other hand, the transition from an initial stage to a steady oscillation with the fixed amplitude relies on the powers of the modulated driving lasers. For example, it is shown from the insets in Fig. 3(a) for $P_{1,\pm 1} = P_{2,\pm 1} = 2.2$ mW that the oscillation amplitude of the transmission coefficient increases up to a maximal value, after which it quickly decreases to a steady-state oscillation with a small amplitude. However, it is shown in Fig. 3(b) for $P_{1,\pm 1} = P_{2,\pm 1} = 2.4$ mW that the nonreciprocal oscillation amplitude gently becomes larger in the initial stage of time evolution, and then it reaches the steady oscillation with a fixed amplitude. When the power of the modulated driving lasers becomes larger, shown in Fig. 3(c) for $P_{1,\pm 1} = P_{2,\pm 1} = 2.6$ mW, the nonreciprocal oscillation amplitude quickly increases and remains at the steady oscillation.

In Figs. 3(a)–3(c), we consider the dependence of the temporal nonreciprocity on the first-order modulated laser with a fixed zeroth-order laser. Now, we shall exhibit the effects of the strength of the zeroth-order laser on the temporal nonreciprocal transmission in the case of a fixed first-order modulated laser, which are illustrated in Fig. 4. From Figs. 4(a)–4(c) with different powers of the zeroth-order laser $P_{1,0} = P_{2,0} = 8, 9$, and 10 mW with the fixed first-order modulated laser, we can see that the oscillation maximum values of the transmission coefficient $T_{1 \rightarrow 2}$ increase while those of the coefficient $T_{2 \rightarrow 1}$ decrease with the zeroth-order laser $P_{1,0}$, which implies that the zeroth-order laser will make the temporal nonreciprocity more effective. Subsequently, we consider the case of the fixed strength ratio of the first-order modulated laser to the zeroth-order laser, i.e., $P_{1,\pm 1}/P_{1,0}$ or $P_{2,\pm 1}/P_{2,0}$. It is shown in Figs. 5(a)–5(c) that the temporal nonreciprocity becomes more effective as the zeroth-order laser $P_{1,0}$ increases.

Now we consider the asymmetric-driven case where $P_{1,0} \neq P_{2,0}$, $P_{1,\pm 1} \neq P_{2,\pm 1}$. In Fig. 6, we plot the transmission coefficients versus the normalized time t/τ when the system is driven by asymmetric-driven lasers. It is found that the temporal nonreciprocity behaves in different patterns when

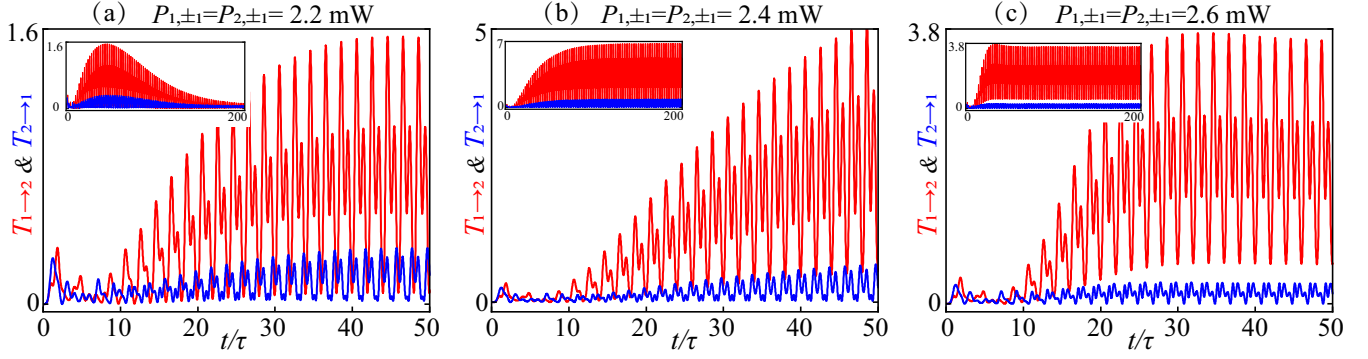


FIG. 3. The temporal nonreciprocal transmission coefficients $T_{1 \rightarrow 2}$ (red solid curves) and $T_{2 \rightarrow 1}$ (blue solid curves) for different power P_1 of the modulation driving laser: (a) $P_{1,\pm 1} = P_{2,\pm 1} = 2.2$ mW, (b) $P_{1,\pm 1} = P_{2,\pm 1} = 2.4$ mW, and (c) $P_{1,\pm 1} = P_{2,\pm 1} = 2.6$ mW. The insets show the corresponding temporal nonreciprocal transmission in the long-time limit $t/\tau \in [0, 200]$. Other parameters are the same as in Fig. 2 except for $\varphi = 0.4\pi$, $P_{1,0} = P_{2,0} = 10$ mW, and $J/\kappa = 1$.

the system is asymmetrically driven by the lasers. Following the comparison of Figs. 6(a)–6(c) where $P_{1,0} = 9.2, 9.5,$ and 9.8 mW with fixed $P_{2,0} = 10$ mW, one can see that the maximal transmission in the steady oscillating regime increases with the zeroth-order driving laser and its time to reach the steady regime becomes longer. On the other hand, the transmission takes on contrary behaviors when the modulated laser $P_{1,\pm 1}$ becomes stronger with the modulated laser $P_{2,\pm 1}$ being fixed at 2.4 mW, which are shown in Figs. 6(d)–6(f).

It is well known that the optomechanically induced nonreciprocity can be generated by the optomechanical-coupling interaction and becomes stronger with the effective optomechanical-coupling interaction enhanced by the driving lasers [34]. This is confirmed by the fact that the transmission coefficients increase with the power $P_{1,0}$ or $P_{2,0}$, which is shown in Figs. 4, 5, and 6(a)–6(c). It takes longer time to reach the larger saturated value (the oscillation maximal value) of the transmission coefficient, shown in Figs. 6(a)–6(c). On the

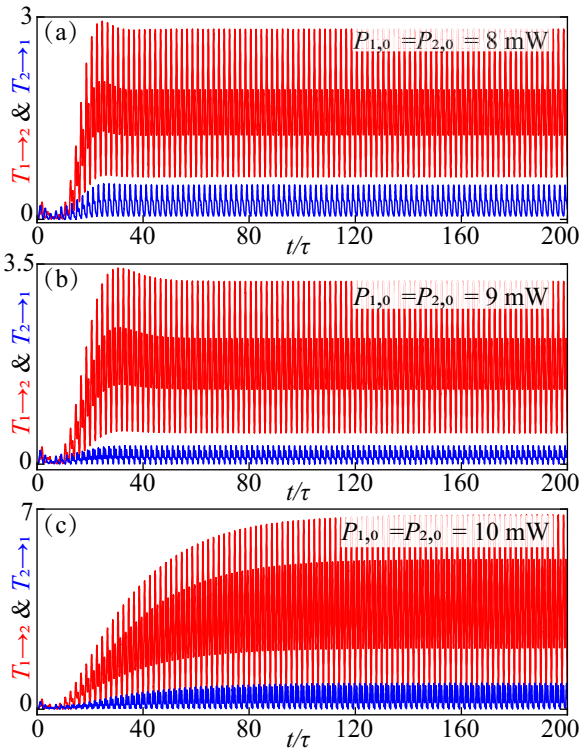


FIG. 4. The temporal transmission coefficients $T_{1 \rightarrow 2}$ (red solid curves) and $T_{2 \rightarrow 1}$ (blue solid curves) at a fixed first-order modulated laser $P_{1,\pm 1} = P_{2,\pm 1} = 2.4$ mW with different powers of the zeroth-order modulated laser: (a) $P_{1,0} = P_{2,0} = 8$ mW, (b) $P_{1,0} = P_{2,0} = 9$ mW, and (c) $P_{1,0} = P_{2,0} = 10$ mW. Other parameters are the same as in Fig. 2 except for $\varphi = 0.4\pi$.

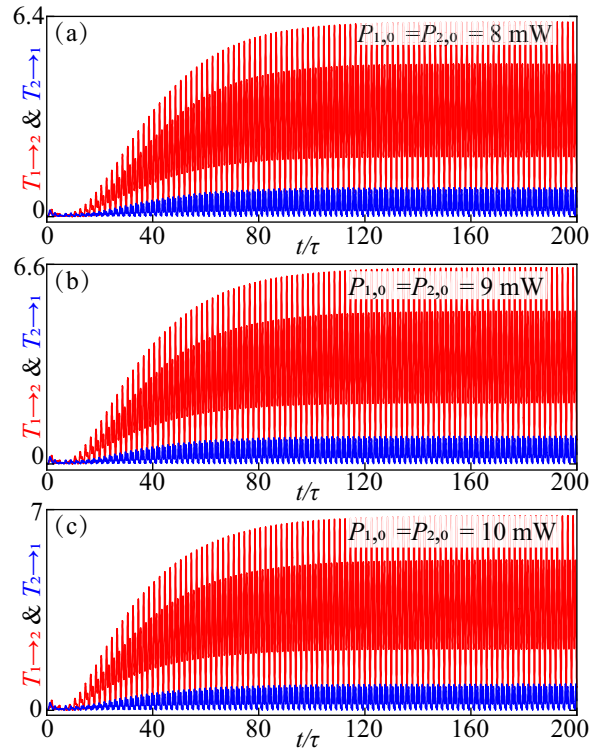


FIG. 5. The temporal transmission coefficients $T_{1 \rightarrow 2}$ (red solid curves) and $T_{2 \rightarrow 1}$ (blue solid curves) at a fixed ratio $P_{1,\pm 1}/P_{1,0} = P_{2,\pm 1}/P_{2,0} = 0.24$ with different power of driving laser: (a) $P_{1,0} = P_{2,0} = 8$ mW, (b) $P_{1,0} = P_{2,0} = 9$ mW, and (c) $P_{1,0} = P_{2,0} = 10$ mW. Other parameters are the same as in Fig. 2 except for $\varphi = 0.4\pi$.

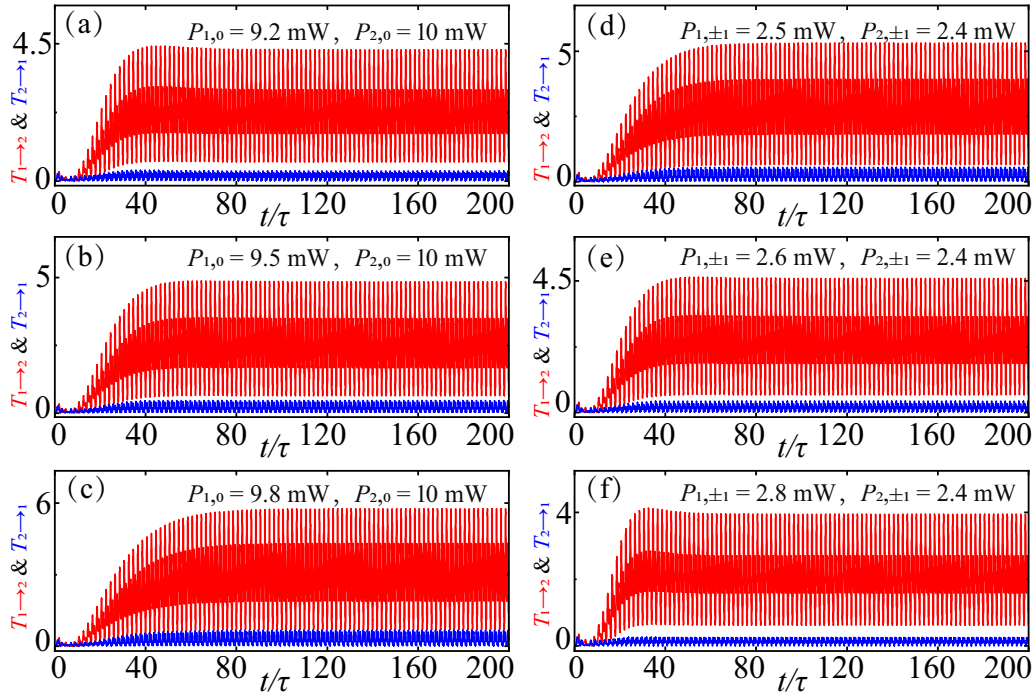


FIG. 6. The temporal transmission coefficients $T_{1 \rightarrow 2}$ (red solid curves) and $T_{2 \rightarrow 1}$ (blue solid curves) for different powers of the zeroth-order driving lasers: $P_{1,0} = 9.2, 9.5,$ and 9.8 mW in (a)–(c) with $P_{1,\pm 1} = P_{2,\pm 1} = 2.4$ mW and $P_{2,0} = 10$ mW, respectively. The temporal transmission coefficients for different powers of the modulated lasers are $P_{1,\pm 1} = 2.5, 2.6,$ and 2.8 mW in (d)–(f) with $P_{2,\pm 1} = 2.4$ mW and $P_{1,0} = P_{2,0} = 10$ mW, respectively. Other parameters are the same as those in Fig. 2 except for $\varphi = 0.4\pi$.

other hand, it is shown in Figs. 6(d)–6(f) that the saturated value of the transmission coefficient decreases with the power $P_{1,\pm 1}$ of the modulated laser, in which it takes shorter time to reach the saturated value. Combining the effects of the powers of the driving lasers and modulated lasers on the transition from an initial stage to a steady oscillation, which play opposite roles in the transition time, the transition time is only determined by the fixed ratio $P_{j,\pm 1}/P_{j,0}$ of the power of the driving laser to that of the modulated laser. This is illustrated in Fig. 5, in which the transition time remains unchanged at a fixed ratio even for different powers of driving and modulated lasers.

V. DEPENDENCE OF TEMPORAL NONRECIPROCAL PHOTON TRANSMISSION ON PHASE DIFFERENCE

Now, we consider the dependence of the temporal nonreciprocal photon transmission on the phase difference φ between the two modulated lasers. It is shown in Fig. 7 that the transmissions coefficients $T_{1 \rightarrow 2}$ and $T_{2 \rightarrow 1}$ evolve within a given time interval $t/\tau \in [560, 570]$ for different phase differences: $\varphi = 0.14\pi$ ($2\pi - 0.14\pi$), 0.28π ($2\pi - 0.28\pi$), and 0.42π ($2\pi - 0.42\pi$). It is clearly seen that the maximal amplitudes of the temporal nonreciprocal transmissions $T_{1 \rightarrow 2}$ and $T_{2 \rightarrow 1}$ strongly rely on the phase difference φ . As illustrated by respective red curves in Figs. 7(a)–7(c), the forward transmission $T_{1 \rightarrow 2} \approx 1.9$ (red curve) for $\varphi = 0.28\pi$ in Fig. 7(b) is obviously larger than $T_{1 \rightarrow 2} \approx 0.86$ (red curve) for $\varphi = 0.14\pi$. Also, it is shown that $T_{1 \rightarrow 2} \approx 13.2$ (red curves) for $\varphi = 0.42\pi$ in Fig. 7(c) is remarkably larger than

$T_{1 \rightarrow 2} \approx 1.9$ (red curve) for $\varphi = 0.28\pi$ in Fig. 7(b). The comparison of Figs. 7(a)–7(c) indicates that the temporal photon nonreciprocity becomes more effective with the phase difference. And the optimal nonreciprocal photon transmission can be realized in the case shown in Fig. 7(c), where the forward photon transmission $T_{1 \rightarrow 2}$ becomes larger than the backward transmission $T_{2 \rightarrow 1}$ within the whole given time interval. Meanwhile, the forward transmission $T_{1 \rightarrow 2} \approx 13.2$ is greatly stronger than the backward transmission $T_{2 \rightarrow 1} \approx 2.1$.

On the other hand, the dominant direction of the temporal nonreciprocal photon transmission can be switched by modulating the phase difference $\varphi \rightarrow 2\pi - \varphi$. Specifically, the forward photon propagation ($T_{1 \rightarrow 2} > T_{2 \rightarrow 1}$) is dominant over the backward photon propagation when the phase difference is located within the regime of $0 < \varphi < \pi$, while the backward dominant propagation ($T_{2 \rightarrow 1} > T_{1 \rightarrow 2}$) occurs when the phase difference is modulated in the regime $\pi < \varphi < 2\pi$. For examples, the forward photon transmission $T_{1 \rightarrow 2}$ becomes larger than the backward transmission $T_{2 \rightarrow 1}$ in Fig. 7(c) for $\varphi = 0.42\pi$, while the backward transmission $T_{2 \rightarrow 1}$ is larger than the forward photon transmission $T_{1 \rightarrow 2}$ in Fig. 7(f) for $\varphi = (2 - 0.42)\pi$.

Additionally, by comparing the temporal nonreciprocities shown in Figs. 7(a)–7(c) for $\varphi = 0.14\pi$, 0.28π , and 0.42π with those in Figs. 7(d)–7(f) for $\varphi = (2 - 0.14)\pi$, $(2 - 0.28)\pi$, and $(2 - 0.42)\pi$, respectively, we can see that the temporal photon nonreciprocity for the phase difference φ is exchange symmetric with that in the case of the phase $2\pi - \varphi$. This can be further demonstrated by the temporal photon transmission shown in Fig. 8, which depicts the temporal

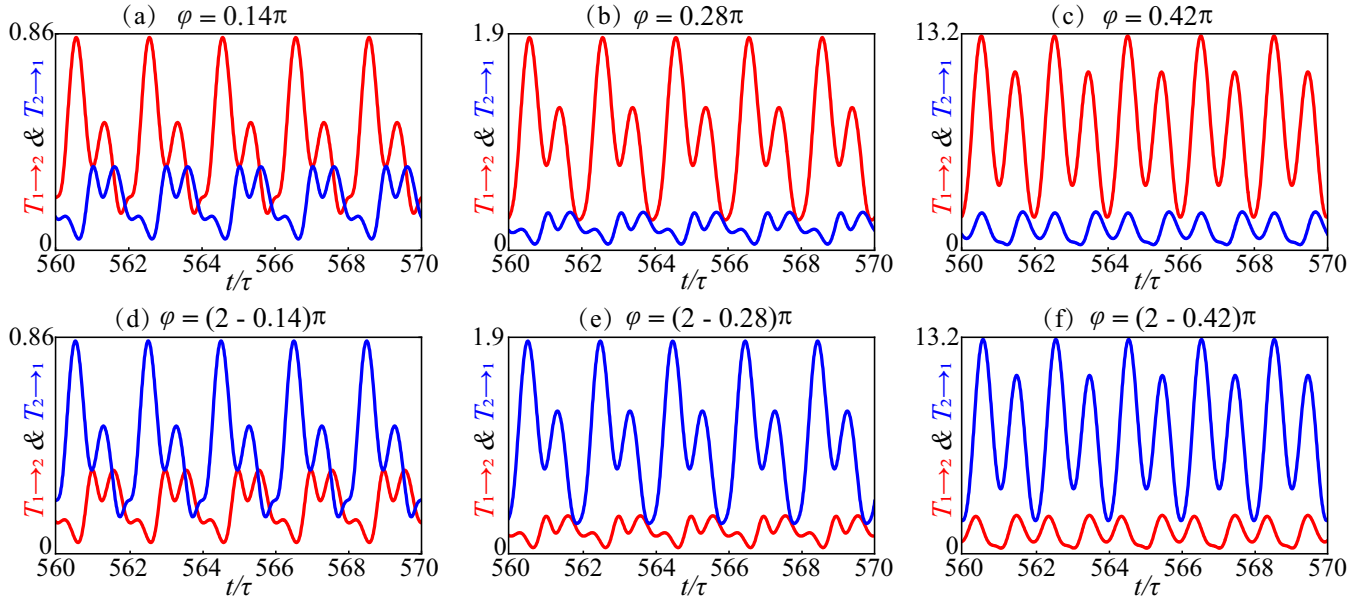


FIG. 7. The temporal transmission coefficients $T_{1 \rightarrow 2}$ (red solid curves) and $T_{2 \rightarrow 1}$ (blue solid curves) for the different phase difference φ : (a) $\varphi = 0.14\pi$, (b) $\varphi = 0.28\pi$, (c) $\varphi = 0.42\pi$, (d) $\varphi = (2 - 0.14)\pi$, (e) $\varphi = (2 - 0.28)\pi$, and (f) $\varphi = (2 - 0.42)\pi$. Other parameters are the same as in Fig. 2 except for $P_{1,\pm 1} = P_{2,\pm 1} = 2.4$ mW and $P_{1,0} = P_{2,0} = 10$ mW.

transmission coefficients $T_{1 \rightarrow 2}$ and $T_{2 \rightarrow 1}$ as functions of the phase φ/π and the times t/τ . Also, we can realize another temporal feature that the dominant photon nonreciprocities in the forward and backward directions are commutative with time evolving, which is shown in Fig. 9.

The isolation parameter $\mathfrak{R} = 10 \log_{10}[T_{1 \rightarrow 2}/T_{2 \rightarrow 1}]$ is mainly determined by the ratio of the transmission coefficients in two opposite directions. The photon nonreciprocity is

produced if $\mathfrak{R} \neq 0$ or $T_{1 \rightarrow 2}(t) \neq T_{2 \rightarrow 1}(t)$. The nonreciprocal photon transmission can be described by only the isolation parameter [96–98]. Next, we compare the effects of periodic and aperiodic pump modulations on the optical nonreciprocity by calculating time evolution of the isolation rate \mathfrak{R} in Fig. 10. It is evident that the isolation rate undergoes oscillations over time in the steady regime when the system is subjected to a periodically modulated laser with ($\Omega \neq 0$), while the rate is steady in the case of aperiodic modulation ($\Omega = 0$), which are shown by the red and blue solid curves in Fig. 10, respectively. Also, it is shown that the isolation rate in the presence of periodic modulation ($\Omega \neq 0$) becomes larger than that in the case of aperiodic modulation.

On the other hand, the isolation parameter \mathfrak{R} is used to illustrate the dependence of the optical nonreciprocity on the modulation frequencies of the driving lasers. We plot the time evolution of the isolation rate for different modulation frequencies in Fig. 11. When the modulation frequencies of

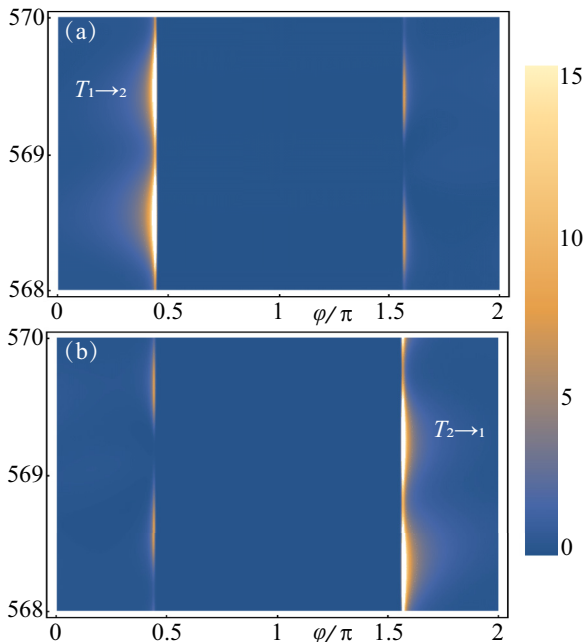


FIG. 8. The temporal transmission coefficients $T_{1 \rightarrow 2}$ and $T_{2 \rightarrow 1}$ as functions of the phase φ/π and the time t/τ . Other parameters are the same as those in Fig. 2.

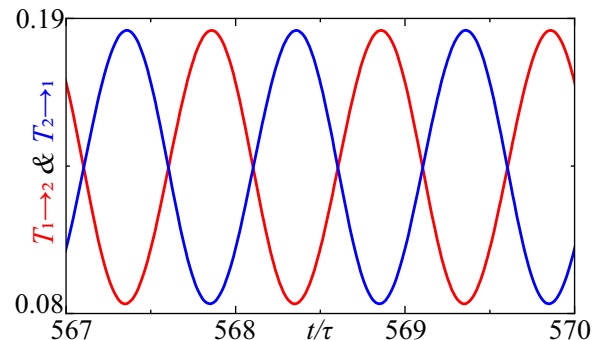


FIG. 9. The time evolution of the temporal transmission coefficients $T_{1 \rightarrow 2}$ (red solid curves) and $T_{2 \rightarrow 1}$ (blue solid curves) for $J/\kappa = 2$, $\varphi = \pi$. Other parameters are the same as those in Fig. 2.

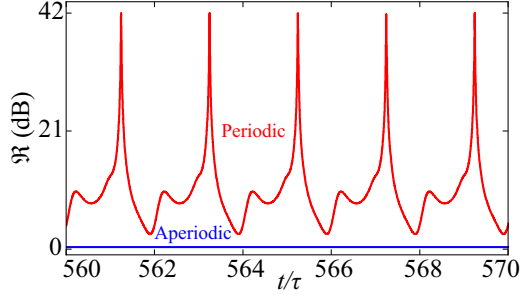


FIG. 10. The scaled isolation parameter \mathfrak{R} as a function of time. Periodic modulation (red curve) can lead to a more significant isolation rate compared to the absence of periodic modulation with $\Omega = 0$ (blue curve). Other parameters are the same as in Fig. 2 in the main text except for $\varphi = 0.42\pi$, $P_{1,0} = P_{2,0} = 10\text{mW}$, and $P_{1,\pm 1} = P_{2,\pm 1} = 2.4\text{mW}$.

the two driving lasers are different, the isolation rate collapses and revives with the periods of $t = 25\tau$ and 50τ , which are respectively shown in Figs. 11(a) and 11(b). However, the isolation rate periodically oscillates in the case of two identical frequencies of the modulated lasers, which is shown in Fig. 11(c). These dynamical behaviors are remarkably analogous to the entanglement beating in a cavity optomechanical system generated by the interference between two waves with slightly different frequencies [80]. Additionally, it is found that the two modulated driving fields with the same frequencies can significantly improve the temporal nonreciprocity

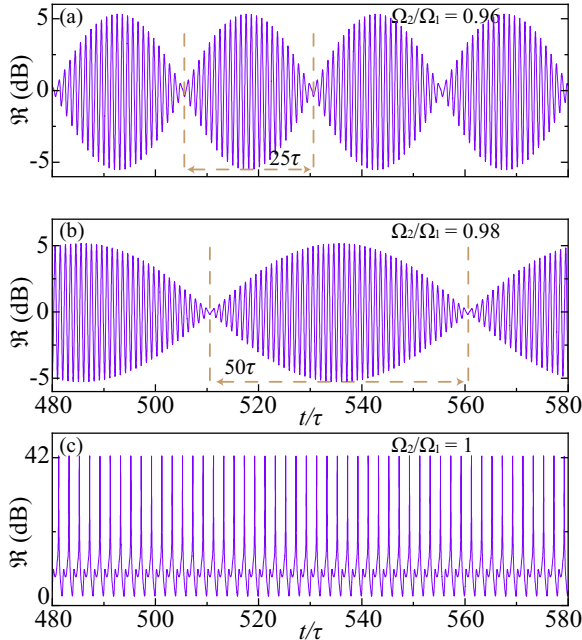


FIG. 11. The time evolutionary isolation rate \mathfrak{R} for different modulation frequencies of the driving lasers: (a) $\Omega_2/\Omega_1 = 0.96$, (b) $\Omega_2/\Omega_1 = 0.98$, and (c) $\Omega_2/\Omega_1 = 1$. Other parameters are the same as in Fig. 2 except for $\varphi = 0.42\pi$, $P_{1,0} = P_{2,0} = 10\text{mW}$, $P_{1,\pm 1} = P_{2,\pm 1} = 2.4\text{mW}$, and $\Omega_1 = \Omega$.

with an increase of the maximum value $\mathfrak{R} = 42$, as shown in Fig. 11(c).

VI. INTERPRETATION OF TRANSMISSION NONRECIPROCIITY

In the above discussion, we have studied the time-dependent nonreciprocal responses by numerical simulation of the output field without any approximation. Now we provide analytical findings to interpret the nonreciprocal transmission behaviors. According to Eq. (9), the cavity fields \hat{a}_1 and \hat{a}_2 to the zeroth order of g can be approximately written as

$$\langle \hat{a}_j(t) \rangle = a_j^{0,0} + a_j^{+1,0} e^{i\Omega t} + a_j^{-1,0} e^{-i\Omega t}, \quad (14)$$

where $j = 1, 2$ and we have omitted the higher-order terms for $n \geq 2$. Correspondingly, the effective optomechanical coupling strength can be effectively expanded as [76,80]

$$G_j(t) = G_{j,0} + G_{j,+1} e^{-i\Omega t} + G_{j,-1} e^{i\Omega t}, \quad (15)$$

where $G_{j,k} = (\frac{1}{\sqrt{2}}) \sum_{l=0}^{\infty} (\sqrt{2}g)^{l+1} a_j^{-k,l}$, with $k = -1, 0, +1$. The cavity is driven in resonance with the red sideband $\Delta_1 = \Delta_2 \approx \omega_m$, and the modulated frequency is set as $\Omega = 2\omega_m$. By transforming the variables as $\tilde{\delta}\hat{b} = \delta\hat{b}e^{i\omega_m t}$, $\tilde{\delta}\hat{a}_1 = \delta\hat{a}_1 e^{i\omega_m t}$, and $\tilde{\delta}\hat{a}_2 = \delta\hat{a}_2 e^{i\omega_m t}$ in the interaction picture at the mechanical frequency ω_m , the corresponding linearized quantum Langevin equations in Eq. (5) read

$$\begin{aligned} \frac{d}{dt} \tilde{\delta}\hat{b} &= -\gamma_m \tilde{\delta}\hat{b} + iG_{1,+1} \tilde{\delta}\hat{a}_1^\dagger + iG_{1,0}^* \tilde{\delta}\hat{a}_1 \\ &\quad - iG_{2,+1} \tilde{\delta}\hat{a}_2^\dagger - iG_{2,0}^* \tilde{\delta}\hat{a}_2 + \sqrt{2\gamma_m} \tilde{b}_{\text{in}}, \\ \frac{d}{dt} \tilde{\delta}\hat{a}_1 &= i\tilde{\delta}\tilde{\delta}\hat{a}_1 - \kappa_1 \tilde{\delta}\hat{a}_1 + iG_{1,0} \tilde{\delta}\hat{b} + iG_{1,+1} \tilde{\delta}\hat{b}^\dagger \\ &\quad - iJ\tilde{\delta}\hat{a}_2 + \sqrt{2\kappa_1} \tilde{a}_{1,\text{in}}, \\ \frac{d}{dt} \tilde{\delta}\hat{a}_2 &= -i\tilde{\delta}\tilde{\delta}\hat{a}_2 - \kappa_2 \tilde{\delta}\hat{a}_2 - iG_{2,0} \tilde{\delta}\hat{b} - iG_{2,+1} \tilde{\delta}\hat{b}^\dagger \\ &\quad - iJ\tilde{\delta}\hat{a}_1 + \sqrt{2\kappa_2} \tilde{a}_{2,\text{in}}. \end{aligned} \quad (16)$$

We can obtain the effectively linearized Hamiltonian corresponding to Eq. (16), which is given by (here $\hbar = 1$)

$$\begin{aligned} \hat{H}_{\text{eff}} &= -\tilde{\delta}\tilde{\delta}\hat{a}_1^\dagger \tilde{\delta}\hat{a}_1 + \tilde{\delta}\tilde{\delta}\hat{a}_2^\dagger \tilde{\delta}\hat{a}_2 + \omega_m \tilde{\delta}\hat{b}^\dagger \tilde{\delta}\hat{b} \\ &\quad + J(\tilde{\delta}\hat{a}_1^\dagger \tilde{\delta}\hat{a}_2 + \tilde{\delta}\hat{a}_1 \tilde{\delta}\hat{a}_2^\dagger) - (G_{1,0} \tilde{\delta}\hat{a}_1^\dagger \tilde{\delta}\hat{b} + G_{1,0}^* \tilde{\delta}\hat{a}_1 \tilde{\delta}\hat{b}^\dagger) \\ &\quad + (G_{2,0} \tilde{\delta}\hat{a}_2^\dagger \tilde{\delta}\hat{b} + G_{2,0}^* \tilde{\delta}\hat{a}_2 \tilde{\delta}\hat{b}^\dagger) - |G_{1,+1}| (\tilde{\delta}\hat{a}_1^\dagger \tilde{\delta}\hat{b}^\dagger + \tilde{\delta}\hat{a}_1 \tilde{\delta}\hat{b}) \\ &\quad + |G_{2,+1}| (\tilde{\delta}\hat{a}_2^\dagger e^{-i\phi} \tilde{\delta}\hat{b}^\dagger + \tilde{\delta}\hat{a}_2 \tilde{\delta}\hat{b} e^{i\phi}), \end{aligned} \quad (17)$$

where $\phi = \phi_2 - \phi_1$, $\phi_1 = \arg[G_{1,+1}]$, and $\phi_2 = \arg[G_{2,+1}]$. The phase of ϕ_1 and ϕ_2 can be controlled by tuning the phases $\varphi_{1(2)}$ of two periodically modulation driving fields. Actually, the phases of ϕ_1 and ϕ_2 have been absorbed by redefining the operators $\tilde{\delta}\hat{a}_i$ and $\tilde{\delta}\hat{b}$, and only the phase difference ϕ between them has physical effects. Similar situations have been extensively studied in cavity optomechanical systems [46,50–52,59].

It is seen that the terms with $G_{j,-1}$ ($j = 1, 2$) and even higher-frequency components are far from the cavity resonance, thus the temporal transmission nonreciprocity of the system will be mainly determined by the two driving components with $G_{j,0}$ and $G_{j,+1}$. Specifically, in the case of resonance with the red-sideband resonance $\Delta_j \approx \omega_m$, there exists the beam-splitter-like part of $\delta\tilde{a}_j^\dagger\delta\tilde{b} + \delta\tilde{a}_j\delta\tilde{b}^\dagger$ and the photon-phonon pair generation one $\delta\tilde{a}_j^\dagger\delta\tilde{b}^\dagger + \delta\tilde{a}_j\delta\tilde{b}$ to dominate the evolution of the system. The interference between the direct coupling of the two cavities and the optomechanical

coupling of the beam-splitter-like part bridged by the mechanical mode leads to the appearance of photon nonreciprocity [34,35], while the photon-phonon pair generation part produces the directional amplification [36,37].

This interference can be shown by the dependence of the photon transmission on the phase difference ϕ between the effective optomechanical coupling probabilities $G_{1,+1}$ and $G_{2,+1}$. In terms of the transmission elements $T_{1\rightarrow 2} = 2\kappa_2|\delta\hat{a}_2/\hat{a}_{1,\text{in}}|^2$ and $T_{2\rightarrow 1} = 2\kappa_1|\delta\hat{a}_1/\hat{a}_{2,\text{in}}|^2$ discussed in the previous section, we get the transmission ratio in the stable regime, which is given by

$$\frac{T_{1\rightarrow 2}}{T_{2\rightarrow 1}} = \left| \frac{|G_{1,0}|^2[\Upsilon_4 - iJ(J\gamma_m + 2|G_{1,+1}G_{2,+1}|\sin\phi)] + \Upsilon_2\{|G_{1,+1}G_{2,+1}|\cos\phi + i[J\gamma_m + |G_{1,+1}G_{2,+1}|\sin\phi]\}}{|G_{1,0}|^2[\Upsilon_4 - iJ(J\gamma_m - 2|G_{1,+1}G_{2,+1}|\sin\phi)] + \Upsilon_2\{|G_{1,+1}G_{2,+1}|\cos\phi + i[J\gamma_m - |G_{1,+1}G_{2,+1}|\sin\phi]\}} \right|^2, \quad (18)$$

where $\Upsilon_1 = 2J|G_{1,+1}G_{2,+1}|\cos\phi + |G_{1,+1}|^2(\bar{\delta} + i\kappa_1) - |G_{2,+1}|^2(\bar{\delta} - i\kappa_1) - i\gamma_m(J^2 + \bar{\delta}^2 + \kappa_1^2)$, $\Upsilon_2 = \Upsilon_1 - 2i\kappa_1|G_{1,0}|^2$, $\Upsilon_3 = (2J + i\kappa_1)(|G_{1,+1}|^2 + |G_{2,+1}|^2) + \bar{\delta}(|G_{1,+1}|^2 - |G_{2,+1}|^2) - i\gamma_m(\bar{\delta}^2 + \kappa_1^2)$, and $\Upsilon_4 = 2|G_{1,0}|^2(J + i\kappa_1) - \Upsilon_3$. Without loss of generality, it is assumed that $G_{1,0} = G_{2,0}$ in the case of symmetric modulations with the red-sideband resonance. If the phase difference is given by $\phi = \pi/2$, we have

$$\frac{T_{1\rightarrow 2}}{T_{2\rightarrow 1}} = \left| \frac{|G_{1,0}|^2[\Upsilon_4 - iJ(\gamma_m J + 2|G_{1,+1}G_{2,+1}|)] + i\Upsilon_2(J\gamma_m + |G_{1,+1}G_{2,+1}|)}{|G_{1,0}|^2[\Upsilon_4 - iJ(\gamma_m J - 2|G_{1,+1}G_{2,+1}|)] + i\Upsilon_2(J\gamma_m - |G_{1,+1}G_{2,+1}|)} \right|^2. \quad (19)$$

For the phase difference $\phi = -\pi/2$, we get

$$\frac{T_{1\rightarrow 2}}{T_{2\rightarrow 1}} = \left| \frac{|G_{1,0}|^2[\Upsilon_4 - iJ(\gamma_m J - 2|G_{1,+1}G_{2,+1}|)] + i\Upsilon_2(J\gamma_m - |G_{1,+1}G_{2,+1}|)}{|G_{1,0}|^2[\Upsilon_4 - iJ(\gamma_m J + 2|G_{1,+1}G_{2,+1}|)] + i\Upsilon_2(J\gamma_m + |G_{1,+1}G_{2,+1}|)} \right|^2. \quad (20)$$

In Fig. 12, we plot the analytical result (green solid line) of the steady transmission ratio $T_{1\rightarrow 2}/T_{2\rightarrow 1}$ and the numerical one (purple solid lines) of the temporal transmission ratio. It is shown that when the temporal transmission ratio reaches its stable regime, the analytical result coincides with the envelope of the numerical results (see green curve in Fig. 12). The nonreciprocal behaviors shown in the above

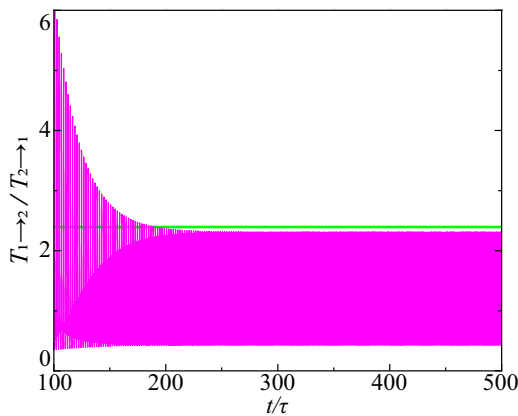


FIG. 12. Temporal evolution and steady value of the transmission ratio $T_{1\rightarrow 2}/T_{2\rightarrow 1}$. The green (purple) solid lines indicate the analytical steady solutions (numerical simulations) for the phase differences $\phi = 0.5\pi$. Other parameters are the same as those in Fig. 2 except for $P_{1,\pm 1} = P_{2,\pm 1} = 2.4$ mW, $P_{1,0} = P_{2,0} = 10$ mW, and $\bar{\delta}/\omega_m = 0$.

discussions can be explained by the interference between the direct coupling of the two cavities and the optomechanical couplings, which are demonstrated by the terms with $J\gamma_m \pm |G_{1,+1}G_{2,+1}|$ and $J\gamma_m \pm 2J|G_{1,+1}G_{2,+1}|$ in Eqs. (19) and (20). When the phase difference is set as $\phi = \pi/2$, the constructive interference between the direct and optomechanical couplings, as shown by the terms with $J\gamma_m + |G_{1,+1}G_{2,+1}|$ and $J\gamma_m + 2J|G_{1,+1}G_{2,+1}|$ in the numerator of Eq. (19), leads the photon propagation from the cavity \hat{a}_1 to \hat{a}_2 dominant over that from the cavity \hat{a}_2 to \hat{a}_1 . Correspondingly, the destructive interference between the two couplings, as described by the terms $J\gamma_m - |G_{1,+1}G_{2,+1}|$ and $J\gamma_m - 2J|G_{1,+1}G_{2,+1}|$ in the denominator of Eq. (19), makes the photon propagation from the cavity \hat{a}_2 to \hat{a}_1 dominant over that from the cavity \hat{a}_1 to \hat{a}_2 . Therefore, we can achieve the temporal nonreciprocal photon transmission and directional amplification in our gently optomechanical system by flexibly modulating the phase difference ϕ , which can be shown in Figs. 7 and 8.

VII. CONCLUSION

In conclusion, we have theoretically studied the temporal nonreciprocal photon transmission in gently modulated three-mode optomechanical systems, in which the two optical modes are simultaneously driven by independent periodically amplitude-modulated lasers. We find that in such a system one can readily achieve the temporal nonreciprocal photon transmission by using the experimentally existing technique.

By elaborately tuning the strengths of modulation lasers, one can effectively improve the nonreciprocal optical transmission and shorten the convergence time to reach an asymptotic oscillating regime. Additionally, it is shown that the degrees of temporal nonreciprocity remarkably rely on the laser amplitude and the phase difference. Therefore, the optomechanical system under the periodically modulated-amplitude driving provides a versatile platform for quantum information processing.

ACKNOWLEDGMENTS

This work was supported partly by National Natural Science Foundation of China (Grants No. 11974009, No. 10647007, and No. 12305023), Chengdu Technological Innovation R&D Project (Grant No. 2021-YF05-02416-GX), and the Science Foundation of Sichuan Province of China (Grant No. 2018JY0180).

APPENDIX: THE EFFECTIVE HAMILTONIAN OF AN OPTOMECHANICS: A MEMBRANE INSIDE A CAVITY

As shown in Fig. 1(b), we assume the suspended membrane with a very small displacement x around its equilibrium position between the two cavities with independent optical modes \hat{a}_1 and \hat{a}_2 . If the membrane moves to the left, the frequency of the \hat{a}_1 cavity induced by the mechanical membrane decreases, e.g., $-\hbar g \hat{a}_1^\dagger \hat{a}_1 (\hat{b} + \hat{b}^\dagger)$, while that of the \hat{a}_2 cavity increases, i.e., $+\hbar g \hat{a}_2^\dagger \hat{a}_2 (\hat{b} + \hat{b}^\dagger)$. If the membrane moves to a certain side of the cavity, the displacement of one optical cavity \hat{a}_1 is decreased ($L - x$), while that of the other cavity \hat{a}_2 is increased ($L + x$) and vice versa [91]. Thus, the Hamiltonian of this three-mode system can be represented

by

$$\hat{H}_0 = \hbar(\omega_{c1} + x\partial\omega_{c1}/\partial x)\hat{a}_1^\dagger\hat{a}_1 + \hbar(\omega_{c2} + x\partial\omega_{c2}/\partial x)\hat{a}_2^\dagger\hat{a}_2 + \hbar\omega_m\hat{b}^\dagger\hat{b} + \hbar J(\hat{a}_1^\dagger\hat{a}_2 + \hat{a}_2^\dagger\hat{a}_1), \quad (\text{A1})$$

where ω_{ci} ($i = 1, 2$) is the resonance frequency of the corresponding cavities with the suspended membrane in the middle ($x = 0$). Here, only the linear order frequency shift remains since $x \ll L$. For simplicity, the resonant frequencies of the two cavities are $\omega_n = n\pi c/L$, where the mode number is $n = 2L/\lambda_n$ with $\lambda_n = 2\pi c/\omega_n$ [99,100]. Then, the frequencies of the two cavities are expanded to the linear order as

$$\omega_{c1}(x) = \frac{2\pi c}{\lambda} = \frac{n\pi c}{L(1-x/L)} \approx \omega_c \left(1 + \frac{x}{L}\right), \quad (\text{A2})$$

$$\omega_{c2}(x) = \frac{2\pi c}{\lambda} = \frac{n\pi c}{L(1+x/L)} \approx \omega_c \left(1 - \frac{x}{L}\right). \quad (\text{A3})$$

The Hamiltonian of the three-mode systems is rewritten as

$$\begin{aligned} \hat{H}_0 &= \hbar\omega_c \left(1 + \frac{x}{L}\right) \hat{a}_1^\dagger \hat{a}_1 + \hbar\omega_c \left(1 - \frac{x}{L}\right) \hat{a}_2^\dagger \hat{a}_2 + \hbar\omega_m \hat{b}^\dagger \hat{b} \\ &+ \hbar J(\hat{a}_1^\dagger \hat{a}_2 + \hat{a}_2^\dagger \hat{a}_1) \\ &= \hbar(\omega_c - g_0 \hat{x}) \hat{a}_1^\dagger \hat{a}_1 + \hbar(\omega_c + g_0 \hat{x}) \hat{a}_2^\dagger \hat{a}_2 \\ &+ \hbar\omega_m \hat{b}^\dagger \hat{b} + \hbar J(\hat{a}_1^\dagger \hat{a}_2 + \hat{a}_2^\dagger \hat{a}_1), \end{aligned} \quad (\text{A4})$$

where $\hat{x} = \sqrt{\hbar/m\omega_m}(\hat{b} + \hat{b}^\dagger)$. Thus, the Hamiltonian of the three-mode optomechanical systems is given by

$$\begin{aligned} \hat{H} &= \hbar\omega_c \hat{a}_1^\dagger \hat{a}_1 + \hbar\omega_c \hat{a}_2^\dagger \hat{a}_2 + \hbar\omega_m \hat{b}^\dagger \hat{b} - \hbar g \hat{a}_1^\dagger \hat{a}_1 (\hat{b} + \hat{b}^\dagger) \\ &+ \hbar g \hat{a}_2^\dagger \hat{a}_2 (\hat{b} + \hat{b}^\dagger) + \hbar J(\hat{a}_1^\dagger \hat{a}_2 + \hat{a}_2^\dagger \hat{a}_1), \end{aligned} \quad (\text{A5})$$

where $g = g_0 \sqrt{\hbar/m\omega_m}$. Accordingly, this three-mode optomechanical system, which can be realized in a membrane-in-the-middle scheme, has been theoretically analyzed [84–86] and experimentally implemented [87–92].

-
- [1] D. Jalas, A. Petrov, M. Eich, W. Freude, S. Fan, Z. Yu, R. Baets, M. Popović, A. Melloni, J. D. Joannopoulos, M. Vanwolleghem, C. R. Doerr, and H. Renner, What is- and what is not-an optical isolator, *Nat. Photon.* **7**, 579 (2013).
- [2] E. Verhagen and A. Alù, Optomechanical nonreciprocity, *Nat. Phys.* **13**, 922 (2017).
- [3] L. Lu, J. D. Joannopoulos, and M. Soljačić, Topological photonics, *Nat. Photon.* **8**, 821 (2014).
- [4] Z. Wang, Y. Chong, J. Joannopoulos, and M. Soljačić, Observation of unidirectional backscattering-immune topological electromagnetic states, *Nature (London)* **461**, 772 (2009).
- [5] M. Hafezi, E. A. Demler, M. D. Lukin, and J. M. Taylor, Robust optical delay lines with topological protection, *Nat. Phys.* **7**, 907 (2011).
- [6] D.-G. Lai, J.-F. Huang, X.-L. Yin, B.-P. Hou, W. Li, D. Vitali, F. Nori, and J.-Q. Liao, Nonreciprocal ground-state cooling of multiple mechanical resonators, *Phys. Rev. A* **102**, 011502(R) (2020).
- [7] H. Dötsch, N. Bahlmann, O. Zhuromskyy, M. Hammer, L. Wilkens, R. Gerhardt, P. Hertel, and A. F. Popkov, Applications of magneto-optical waveguides in integrated optics: Review, *J. Opt. Soc. Am. B* **22**, 240 (2005).
- [8] K. Fang, Z. Yu, and S. Fan, Photonic Aharonov-Bohm effect based on dynamic modulation, *Phys. Rev. Lett.* **108**, 153901 (2012).
- [9] E. Li, B. Eggleton, K. Fang, and S. Fan, Photonic Aharonov-Bohm effect in photon-phonon interactions, *Nat. Commun.* **5**, 3225 (2014).
- [10] A. Mock, D. Sounas, and A. Alù, Tunable orbital angular momentum radiation from angular-momentum-biased microcavities, *Phys. Rev. Lett.* **121**, 103901 (2017).
- [11] D. L. Sounas and A. Alù, Angular-momentum-biased nanorings to realize magnetic-free integrated optical isolation, *ACS Photonics* **1**, 198 (2014).
- [12] P. Lodahl, S. Mahmoodian, S. Stobbe, A. Rauschenbeutel, P. Schneeweiss, J. Volz, H. Pichler, and P. Zoller, Chiral quantum optics, *Nature (London)* **541**, 473 (2017).
- [13] K. Xia, F. Nori, and M. Xiao, Cavity-free optical isolators and circulators using a chiral cross-Kerr nonlinearity, *Phys. Rev. Lett.* **121**, 203602 (2018).

- [14] L. Tang, J. Tang, W. Zhang, G. Lu, H. Zhang, Y. Zhang, K. Xia, and M. Xiao, On-chip chiral single-photon interface: Isolation and unidirectional emission, *Phys. Rev. A* **99**, 043833 (2019).
- [15] L. Tang, J. Tang, M. Chen, F. Nori, M. Xiao, and K. Xia, Quantum squeezing induced optical nonreciprocity, *Phys. Rev. Lett.* **128**, 083604 (2022).
- [16] Q. Liu, S. Li, B. Wang, S. Ke, C. Qin, K. Wang, W. Liu, D. Gao, P. Berini, and P. Lu, Efficient mode transfer on a compact silicon chip by encircling moving exceptional points, *Phys. Rev. Lett.* **124**, 153903 (2020).
- [17] Q. Liu, J. Liu, D. Zhao, and B. Wang, On-chip experiment for chiral mode transfer without enclosing an exceptional point, *Phys. Rev. A* **103**, 023531 (2021).
- [18] Y. Shi, Z. Yu, and S. Fan, Limitations of nonlinear optical isolators due to dynamic reciprocity, *Nat. Photon.* **9**, 388 (2015).
- [19] A. R. Hamann, C. Müller, M. Jerger, M. Zanner, J. Combes, M. Pletyukhov, M. Weides, T. M. Stace, and A. Fedorov, Nonreciprocity realized with quantum nonlinearity, *Phys. Rev. Lett.* **121**, 123601 (2018).
- [20] S. R. K. Rodriguez, V. Goblot, N. Carlon Zambon, A. Amo, and J. Bloch, Nonreciprocity and zero reflection in nonlinear cavities with tailored loss, *Phys. Rev. A* **99**, 013851 (2019).
- [21] X.-W. Xu, Y. Li, B. Li, H. Jing, and A.-X. Chen, Nonreciprocity via nonlinearity and synthetic magnetism, *Phys. Rev. Appl.* **13**, 044070 (2020).
- [22] H. Ramezani, T. Kottos, R. El-Ganainy, and D. N. Christodoulides, Unidirectional nonlinear \mathcal{PT} -symmetric optical structures, *Phys. Rev. A* **82**, 043803 (2010).
- [23] C. Eüter, K. G. Makris, R. El-Ganainy, D. N. Christodoulides, M. Segev, and D. Kip, Observation of parity-time symmetry in optics, *Nat. Phys.* **6**, 192 (2010).
- [24] B. Peng, S. K. Özdemir, F. Lei, F. Monifi, M. Gianfreda, G. L. Long, S. H. Fan, F. Nori, C. M. Bender, and L. Yang, Parity-time-symmetric whispering-gallery microcavities, *Nat. Phys.* **10**, 394 (2014).
- [25] L. Chang, X. Jiang, S. Hua, C. Yang, J. Wen, L. Jiang, G. Li, G. Wang, and M. Xiao, Parity-time symmetry and variable optical isolation in active-passive-coupled microresonators, *Nat. Photon.* **8**, 524 (2014).
- [26] B. He, L. Yang, X. S. Jiang, and M. Xiao, Transmission nonreciprocity in a mutually coupled circulating structure, *Phys. Rev. Lett.* **120**, 203904 (2018).
- [27] M. Aspelmeyer, T. J. Kippenberg, and F. Marquardt, Cavity optomechanics, *Rev. Mod. Phys.* **86**, 1391 (2014).
- [28] P. Meystre, A short walk through quantum optomechanics, *Ann. Phys. (NY)* **525**, 215 (2013).
- [29] T. J. Kippenberg and K. J. Vahala, Cavity opto-mechanics, *Opt. Express* **15**, 17172 (2007).
- [30] S. Weis, R. Rivière, S. Deléglise, E. Gavartin, O. Arcizet, A. Schliesser, and T. J. Kippenberg, Optomechanically induced transparency, *Science* **330**, 1520 (2010).
- [31] A. H. Safavi-Naeini, T. P. Mayer Alegre, J. Chan, M. Eichenfield, M. Winger, Q. Lin, J. T. Hill, D. E. Chang, and O. Painter, Electromagnetically induced transparency and slow light with optomechanics, *Nature (London)* **472**, 69 (2011).
- [32] B. P. Hou, L. F. Wei, and S. J. Wang, Optomechanically induced transparency and absorption in hybridized optomechanical systems, *Phys. Rev. A* **92**, 033829 (2015).
- [33] D.-G. Lai, X. Wang, W. Qin, B.-P. Hou, F. Nori, and J.-Q. Liao, Tunable optomechanically induced transparency by controlling the dark-mode effect, *Phys. Rev. A* **102**, 023707 (2020).
- [34] Z. Shen, Y.-L. Zhang, Y. Chen, C.-L. Zou, Y.-F. Xiao, X.-B. Zou, F.-W. Sun, G.-C. Guo, and C.-H. Dong, Experimental realization of optomechanically induced non-reciprocity, *Nat. Photonics* **10**, 657 (2016).
- [35] Z. Shen, Y.-L. Zhang, Y. Chen, F.-W. Sun, X.-B. Zou, G.-C. Guo, C.-L. Zou, and C.-H. Dong, Reconfigurable optomechanical circulator and directional amplifier, *Nat. Commun.* **9**, 1797 (2018).
- [36] C. Jiang, L. N. Song, and Y. Li, Directional phase-sensitive amplifier between microwave and optical photons, *Phys. Rev. A* **99**, 023823 (2019).
- [37] D. Malz, L. D. Tóth, N. R. Bernier, A. K. Feofanov, T. J. Kippenberg, and A. Nunnenkamp, Quantum-limited directional amplifiers with optomechanics, *Phys. Rev. Lett.* **120**, 023601 (2018).
- [38] F. Marquardt, J. P. Chen, A. A. Clerk, and S. M. Girvin, Quantum theory of cavity-assisted sideband cooling of mechanical motion, *Phys. Rev. Lett.* **99**, 093902 (2007).
- [39] J. D. Teufel, T. Donner, D. Li, J. W. Harlow, M. S. Allman, K. Cicak, A. J. Sirois, J. D. Whittaker, K. W. Lehnert, and R. W. Simmonds, Sideband cooling of micromechanical motion to the quantum ground state, *Nature (London)* **475**, 359 (2011).
- [40] H. Xu, L. Jiang, A. A. Clerk, and J. G. E. Harris, Nonreciprocal control and cooling of phonon modes in an optomechanical system, *Nature (London)* **568**, 65 (2019).
- [41] D.-G. Lai, F. Zou, B.-P. Hou, Y.-F. Xiao, and J.-Q. Liao, Simultaneous cooling of coupled mechanical resonators in cavity optomechanics, *Phys. Rev. A* **98**, 023860 (2018).
- [42] D.-G. Lai, W. Qin, B.-P. Hou, A. Miranowicz, and F. Nori, Significant enhancement in refrigeration and entanglement in auxiliary-cavity-assisted optomechanical systems, *Phys. Rev. A* **104**, 043521 (2021).
- [43] S. Manipatruni, J. T. Robinson, and M. Lipson, Optical nonreciprocity in optomechanical structures, *Phys. Rev. Lett.* **102**, 213903 (2009).
- [44] M.-A. Miri, F. Ruesink, E. Verhagen, and A. Alù, Optical nonreciprocity based on optomechanical coupling, *Phys. Rev. Appl.* **7**, 064014 (2017).
- [45] L. Tian and Z. Li, Nonreciprocal quantum-state conversion between microwave and optical photons, *Phys. Rev. A* **96**, 013808 (2017).
- [46] X. W. Xu and Y. Li, Optical nonreciprocity and optomechanical circulator in three-mode optomechanical systems, *Phys. Rev. A* **91**, 053854 (2015).
- [47] Z. X. Tang and X. W. Xu, Thermal-noise cancellation for optomechanically induced nonreciprocity in a whispering-gallery-mode microresonator, *Phys. Rev. Appl.* **19**, 034093 (2023).
- [48] F. Ruesink, M.-A. Miri, A. Alù, and E. Verhagen, Nonreciprocity and magnetic-free isolation based on optomechanical interactions, *Nat. Commun.* **7**, 13662 (2016).
- [49] M. Hafezi and P. Rabl, Optomechanically induced nonreciprocity in microring resonators, *Opt. Express* **20**, 7672 (2012).
- [50] G. Li, X. Xiao, Y. Li, and X. Wang, Tunable optical nonreciprocity and a phonon-photon router in an optomechanical

- system with coupled mechanical and optical modes, *Phys. Rev. A* **97**, 023801 (2018).
- [51] N. R. Bernier, L. D. Tóth, A. Koottandavida, M. A. Ioannou, D. Malz, A. Nunnenkamp, A. K. Feofanov, and T. J. Kippenberg, Nonreciprocal reconfigurable microwave optomechanical circuit, *Nat. Commun.* **8**, 604 (2017).
- [52] S. Barzanjeh, M. Wulf, M. Peruzzo, M. Kalaee, P. B. Dieterle, O. Painter, and J. M. Fink, Mechanical on-chip microwave circulator, *Nat. Commun.* **8**, 953 (2017).
- [53] Z. Shen, Y.-L. Zhang, Y. Chen, Y.-F. Xiao, C.-L. Zou, G.-C. Guo, and C.-H. Dong, Nonreciprocal frequency conversion and mode routing in a microresonator, *Phys. Rev. Lett.* **130**, 013601 (2023).
- [54] D.-G. Lai, J.-Q. Liao, A. Miranowicz, and F. Nori, Noise-tolerant optomechanical entanglement via synthetic magnetism, *Phys. Rev. Lett.* **129**, 063602 (2022).
- [55] B. Tang, B.-P. Hou, X.-H. Zhao, Y.-B. Qian, and D.-G. Lai, Optical nonreciprocity in a three-mode optomechanical system within a common reservoir, *J. Opt. Soc. Am. B* **37**, 1550 (2020).
- [56] L. Mercier de Lépinay, E. Damskågg, C. F. Ockeloen-Korppi, and M. A. Sillanpää, Realization of directional amplification in a microwave optomechanical device, *Phys. Rev. Appl.* **11**, 034027 (2019).
- [57] K. Fang, J. Luo, A. Metelmann, M. H. Matheny, F. Marquardt, A. A. Clerk, and O. Painter, Generalized non-reciprocity in an optomechanical circuit via synthetic magnetism and reservoir engineering, *Nat. Phys.* **13**, 465 (2017).
- [58] A. Metelmann and A. A. Clerk, Nonreciprocal photon transmission and amplification via reservoir engineering, *Phys. Rev. X* **5**, 021025 (2015).
- [59] Y.-B. Qian, D.-G. Lai, M.-R. Chen, and B.-P. Hou, Nonreciprocal photon transmission with quantum noise reduction via cross-Kerr nonlinearity, *Phys. Rev. A* **104**, 033705 (2021).
- [60] A. Metelmann and A. A. Clerk, Quantum-limited amplification via reservoir engineering, *Phys. Rev. Lett.* **112**, 133904 (2014).
- [61] S. Maayani, R. Dahan, Y. Kligerman, E. Moses, A. U. Hassan, H. Jing, F. Nori, D. N. Christodoulides, and T. Carmon, Flying couplers above spinning resonators generate irreversible refraction, *Nature (London)* **558**, 569 (2018).
- [62] R. Huang, A. Miranowicz, J.-Q. Liao, F. Nori, and H. Jing, Nonreciprocal photon blockade, *Phys. Rev. Lett.* **121**, 153601 (2018).
- [63] Y.-F. Jiao, S.-D. Zhang, Y.-L. Zhang, A. Miranowicz, L.-M. Kuang, and H. Jing, Nonreciprocal optomechanical entanglement against backscattering losses, *Phys. Rev. Lett.* **125**, 143605 (2020).
- [64] A. A. Clerk, Introduction to quantum non-reciprocal interactions: From non-Hermitian Hamiltonians to quantum master equations and quantum feedforward schemes, *SciPost Phys. Lect. Notes* **44** (2022).
- [65] N. Estep, D. Sounas, J. Soric, and A. Alù, Magnetic-free non-reciprocity and isolation based on parametrically modulated coupled-resonator loops, *Nat. Phys.* **10**, 923 (2014).
- [66] T. T. Koutserimpas and R. Fleury, Nonreciprocal gain in non-Hermitian time-Floquet systems, *Phys. Rev. Lett.* **120**, 087401 (2018).
- [67] A. Mari and J. Eisert, Gently modulating optomechanical systems, *Phys. Rev. Lett.* **103**, 213603 (2009).
- [68] I. Pietikäinen, O. Černotik, and R. Filip, Combining Floquet and Lyapunov techniques for time-dependent problems in optomechanics and electromechanics, *New J. Phys.* **22**, 063019 (2020).
- [69] L. Mercadé, K. Pelka, R. Burgwal, A. Xuereb, A. Martínez, and E. Verhagen, Floquet phonon lasing in multimode optomechanical systems, *Phys. Rev. Lett.* **127**, 073601 (2021).
- [70] K. Pelka, G. Madiot, R. Braive, and A. Xuereb, Floquet control of optomechanical bistability in multimode systems, *Phys. Rev. Lett.* **129**, 123603 (2022).
- [71] G. Madiot, S. Barbay, and R. Braive, Vibrational resonance amplification in a thermo-optic optomechanical nanocavity, *Nano. Lett.* **21**, 8311 (2021).
- [72] Y. Zhang and G. Chen, Nonlinear effects in a Floquet-driven optomechanical system, *Phys. Rev. A* **107**, 023520 (2023).
- [73] H. Xiong, L. G. Si, X. Y. Lü, X. X. Yang, and Y. Wu, Carrier-envelope phase-dependent effect of high-order sideband generation in ultrafast driven optomechanical system, *Opt. Lett.* **38**, 353 (2013).
- [74] J.-H. Liu, Y.-F. Yu, J.-D. Wang, and Z.-M. Zhang, High-efficiency generation of flat high-order sidebands in a gently modulating optomechanical system, *Ann. Phys. (NY)* **534**, 2100359 (2022).
- [75] A. Szorkovszky, A. C. Doherty, G. I. Harris, and W. P. Bowen, Mechanical squeezing via parametric amplification and weak measurement, *Phys. Rev. Lett.* **107**, 213603 (2011).
- [76] C. S. Hu, Z. B. Yang, H. Z. Wu, Y. Li, and S. B. Zheng, Twofold mechanical squeezing in a cavity optomechanical system, *Phys. Rev. A* **98**, 023807 (2018).
- [77] A. Farace and V. Giovannetti, Enhancing quantum effects via periodic modulations in optomechanical systems, *Phys. Rev. A* **86**, 013820 (2012).
- [78] C.-S. Hu, L.-T. Shen, Z.-B. Yang, H. Wu, Y. Li, and S.-B. Zheng, Manifestation of classical nonlinear dynamics in optomechanical entanglement with a parametric amplifier, *Phys. Rev. A* **100**, 043824 (2019).
- [79] C.-G. Liao, H. Xie, X. Shang, Z.-H. Chen, and X.-M. Lin, Enhancement of steady-state bosonic squeezing and entanglement in a dissipative optomechanical system, *Opt. Express* **26**, 13783 (2018).
- [80] C.-S. Hu, Z.-Q. Liu, Y. Liu, L.-T. Shen, H. Wu, and S.-B. Zheng, Entanglement beating in a cavity optomechanical system under two-field driving, *Phys. Rev. A* **101**, 033810 (2020).
- [81] W.-J. Zhang, Y. Zhang, Q. Guo, A.-P. Liu, G. Li, and T. Zhang, Strong mechanical squeezing and optomechanical entanglement in a dissipative double-cavity system via pump modulation, *Phys. Rev. A* **104**, 053506 (2021).
- [82] L. Ying, Y.-C. Lai, and C. Grebogi, Quantum manifestation of a synchronization transition in optomechanical systems, *Phys. Rev. A* **90**, 053810 (2014).
- [83] H. Lira, Z. Yu, S. Fan, and M. Lipson, Electrically driven nonreciprocity induced by interband photonic transition on a silicon chip, *Phys. Rev. Lett.* **109**, 033901 (2012).
- [84] H. K. Cheung and C. K. Law, Nonadiabatic optomechanical Hamiltonian of a moving dielectric membrane in a cavity, *Phys. Rev. A* **84**, 023812 (2011).
- [85] C. Biancofiore, M. Karuza, M. Galassi, R. Natali, P. Tombesi, G. D. Giuseppe, and D. Vitali, Quantum dynamics of an optical cavity coupled to a thin semitransparent membrane: Effect of membrane absorption, *Phys. Rev. A* **84**, 033814 (2011).

- [86] R. X. Chen, L. T. Shen, Z. B. Yang, H. Z. Wu, and S. B. Zheng, Enhancement of entanglement in distant mechanical vibrations via modulation in a coupled optomechanical system, *Phys. Rev. A* **89**, 023843 (2014).
- [87] J. C. Sankey, C. Yang, B. M. Zwickl, A. M. Jayich, and J. G. Harris, Strong and tunable nonlinear optomechanical coupling in a low-loss system, *Nat. Phys.* **6**, 707 (2010).
- [88] M. Karuza, C. Biancofiore, M. Bawaj, C. Molinelli, M. Galassi, R. Natali, P. Tombesi, G. D. Giuseppe, and D. Vitali, Optomechanically induced transparency in a membrane-in-the-middle setup at room temperature, *Phys. Rev. A* **88**, 013804 (2013).
- [89] R. W. Andrews, R. W. Peterson, T. P. Purdy, K. Cicak, R. W. Simmonds, C. A. Regal, and K. W. Lehnert, Bidirectional and efficient conversion between microwave and optical light, *Nat. Phys.* **10**, 321 (2014).
- [90] D. Lee, M. Underwood, D. Mason, A. B. Shkarin, S. W. Hoch, and J. G. E. Harris, Multimode optomechanical dynamics in a cavity with avoided crossings, *Nat. Commun.* **6**, 6232 (2015).
- [91] A. M. Jayich, J. C. Sankey, B. M. Zwickl, C. Yang, J. D. Thompson, S. M. Girvin, A. A. Clerk, F. Marquardt, and J. G. E. Harris, Dispersive optomechanics: a membrane inside a cavity, *New J. Phys.* **10**, 095008 (2008).
- [92] J. D. Thompson, B. M. Zwickl, A. M. Jayich, F. Marquardt, S. M. Girvin, and J. G. E. Harris, Strong dispersive coupling of a high-finesse cavity to a micromechanical membrane, *Nature (London)* **452**, 72 (2008).
- [93] G. S. Agarwal and S. Huang, Optomechanical systems as single photon routers, *Phys. Rev. A* **85**, 021801(R) (2012).
- [94] E. X. DeJesus and C. Kaufman, Routh-Hurwitz criterion in the examination of eigenvalues of a system of nonlinear ordinary differential equations, *Phys. Rev. A* **35**, 5288 (1987).
- [95] C. W. Gardiner and M. J. Collett, Input and output in damped quantum systems: Quantum stochastic differential equations and the master equation, *Phys. Rev. A* **31**, 3761 (1985).
- [96] Y. Jiang, S. Maayani, T. Carmon, F. Nori, and H. Jing, Nonreciprocal phonon laser, *Phys. Rev. Appl.* **10**, 064037 (2018).
- [97] S. Hua, J. Wen, X. Jiang, Q. Hua, L. Jiang, and M. Xiao, Demonstration of a chip-based optical isolator with parametric amplification, *Nat. Commun.* **7**, 13657 (2016).
- [98] Y. Xu, J.-Y. Liu, W. Liu, and Y.-F. Xiao, Nonreciprocal phonon laser in a spinning microwave magnomechanical system, *Phys. Rev. A* **103**, 053501 (2021).
- [99] M. Bhattacharya, H. Uys, and P. Meystre, Optomechanical trapping and cooling of partially reflective mirrors, *Phys. Rev. A* **77**, 033819 (2008).
- [100] C. K. Law, Interaction between a moving mirror and radiation pressure: A Hamiltonian formulation, *Phys. Rev. A* **51**, 2537 (1995).